

## Electronic Supplementary Information

*for*

### **1,3,5,7-Tetrakis(tetrazol-5-yl)-adamantane: the smallest tetrahedral tetrazole-functionalized ligand and its complexes formed by reaction with anhydrous M(II)Cl<sub>2</sub> (M= Mn, Cu, Zn, Cd)**

*by*

Ishtvan Boldog,<sup>\*a,b</sup> Konstantin V. Domasevitch,<sup>b</sup> Joaquín Sanchiz,<sup>c</sup> Peter Mayer,<sup>d</sup> Christoph Janiak<sup>\*a</sup>

<sup>a</sup> Institut für Anorganische Chemie und Strukturchemie, Universität Düsseldorf, Universitätsstr. 1, D-40225 Düsseldorf, Germany

<sup>b</sup> Inorganic Chemistry Department, Taras Shevchenko National University of Kiev, Vladimirskaya Street 64, Kiev 01033, Ukraine

<sup>c</sup> Departamento de Química Inorgánica, Universidad de La Laguna, c/o Astrofísico Francisco Sánchez s/n, 38206 La Laguna (Tenerife), Spain

<sup>d</sup> Department Chemie, Ludwig-Maximilians-Universität München, Butenandtstr. 5-13, Haus D, D-81377 München, Germany

## Table of contents

NMR.....	1
Notes upon single crystal XRD experiments .....	2
[Cu <sub>4</sub> Cl <sub>4</sub> L(DMF) <sub>5</sub> ] · DMF, 1 .....	2
[Cd <sub>4</sub> Cl <sub>4</sub> L(DMF) <sub>7</sub> ] · DMF, 2 .....	5
[Zn <sub>3</sub> Cl <sub>2</sub> L(DMF) <sub>4</sub> ] · 2DMF, 3 .....	8
[Mn <sub>2</sub> L(DMF) <sub>2</sub> (MeOH) <sub>4</sub> ] DMF · 2MeOH · 2H <sub>2</sub> O, 4 .....	10
<i>Estimation of the solvent content based on the structural data</i> .....	12
TGA.....	14
IR spectroscopy.....	21
Powder XRD measurements .....	23
Sorption studies.....	30
Database .....	43

# NMR

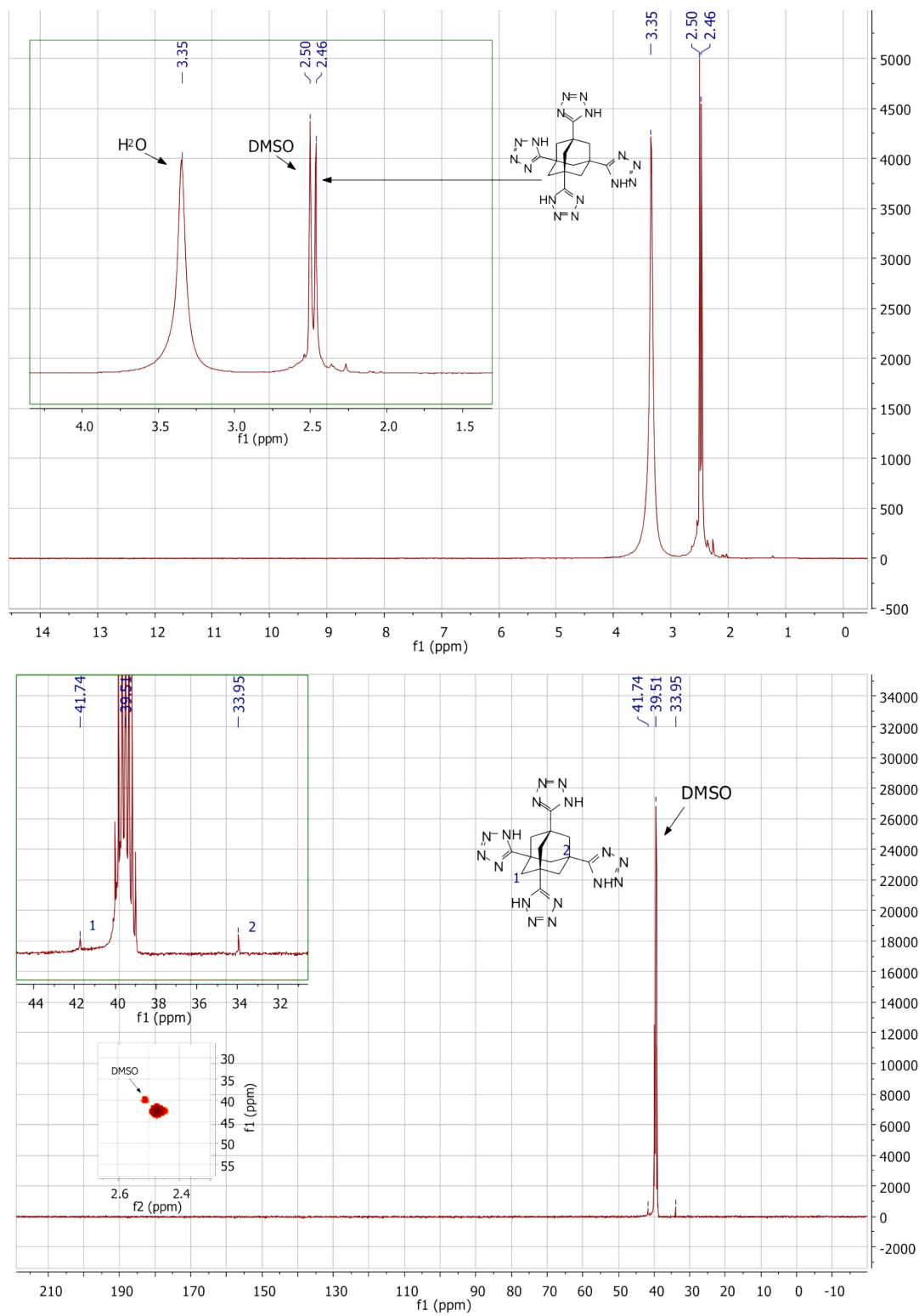
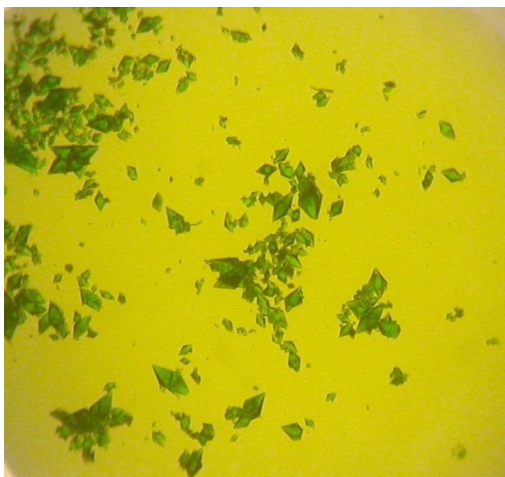


Fig. S2  $^1H$  and  $^{13}C$  spectra of  $H_4L \cdot 3H_2O$  ( $H_4L$  = 1,3,5,7-tetrakis-(tetrazol-5-yl)adamantane).



*Notes upon single crystal XRD experiments*

$[\text{Cu}_4\text{Cl}_4\text{L}(\text{DMF})_5] \cdot \text{DMF}$ , **1**



**Fig. S3.** Octahedral monocrystals of **1** in mother solution.

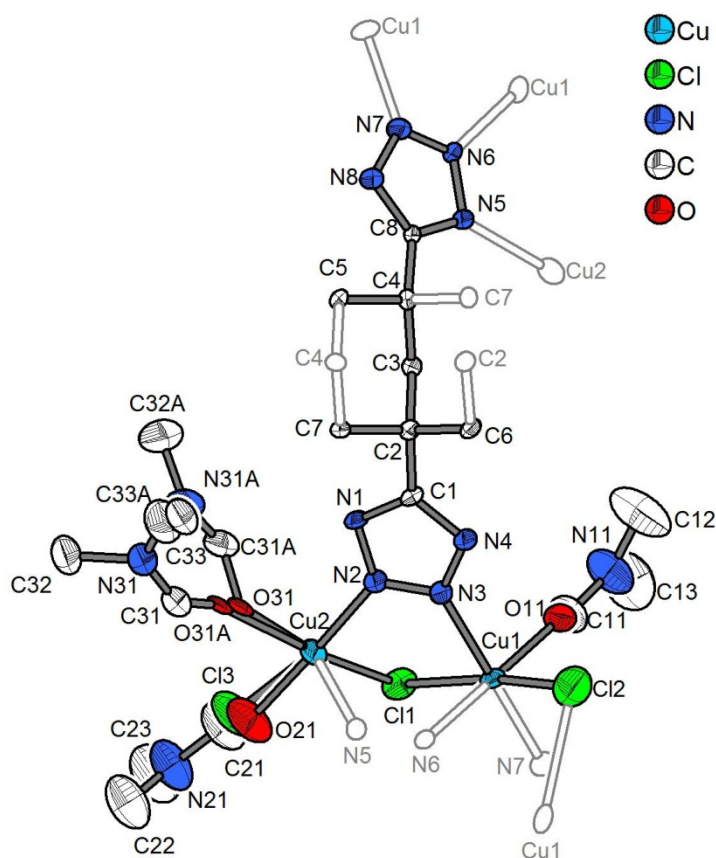


Fig. S4. ORTEP drawing of **1** at 50% probability level. The bound symmetry equivalents are shown as empty ellipsoids with dark gray outline. Two coordinated DMF molecules are positionally disordered. Cl3 and O21 is a pair of occupationally disordered atoms: the respective molecular moieties, represented by the coordinated DMF molecule and the chloride anion have an occupancy factor of 0.5. C32B and C41A are components of the non-coordinated DMF molecule. Hydrogen atoms are not shown for clarity.

The structure features positional disorder of a terminally coordinated Cl3 atom and an N,N-dimethylformamide molecule (0.5:0.5 ratio). The validity of that disorder is proven by high residual electronic density and high anisotropy of localized Cl3 or O21 atoms, when refined within a non-disordered model. Occupancy factor of 0.5 for Cl3 atom is also demanded by the electroneutrality of the molecular formula. The thermal displacement parameters of the disordered atoms were equated by the EADP restraint (SHELXL).

The other coordinated DMF molecules are also disordered. Their geometry was restrained using the next standard values for bond lengths: C-O 1.23(1); C(O)-N 1.31(1); N-CH<sub>3</sub> 1.47(1). The C(O)-NMe<sub>2</sub> fragment was restrained to be co-planar within 0.01 Å standard deviation (FLAT). A set of similarity restraints (SADI / DELU) for the thermal displacement

factors of the atoms constituting the disordered DMF molecules were also applied. The H-atoms of the disordered DMF molecules were added geometrically and refined using the appropriate constraint for the idealized geometry.

There is one highly disordered DMF molecule per formula unit residing in the pores of the compound. It was not feasible / reasonable to resolve the disorder due to its high complexity, hence it was removed using the SQUEEZE (PLATON) routine.

**Tab. S1** Selected bond lengths (Å) and angles (°) involving metal atoms for [Cu<sub>4</sub>Cl<sub>4</sub>L(DMF)<sub>5</sub>] · DMF, **1**

Cu1-O11	1.978(5)	O21-Cu2-N2	175.9(8)
Cu1-N3	1.990(5)	O21-Cu2-O31	93.1(9)
Cu1-N7#a	2.002(5)	N2-Cu2-O31	83.2(3)
Cu1-N6#b	2.033(5)	O21-Cu2-O31A	81.2(9)
Cu1-Cl2	2.599(3)	N2-Cu2-O31A	95.8(3)
Cu1-C11	2.7354(18)	O31-Cu2-O31A	19.2(4)
Cu2-O21	1.919(16)	O21-Cu2-Cl3	12.0(7)
Cu2-N2	1.993(5)	N2-Cu2-Cl3	169.1(2)
Cu2-O31	2.033(9)	O31-Cu2-Cl3	92.5(3)
Cu2-O31A	2.108(9)	O31A-Cu2-Cl3	77.8(4)
Cu2-Cl3	2.213(6)	O21-Cu2-Cl1	93.8(8)
Cu2-Cl1	2.283(2)	N2-Cu2-Cl1	90.03(16)
Cu2-N5#b	2.466(5)	O31-Cu2-Cl1	170.1(3)
Cl2-Cu1#c	2.599(3)	O31A-Cu2-Cl1	157.4(4)
N5-Cu2#d	2.466(5)	Cl3-Cu2-Cl1	92.8(2)
N6-Cu1#d	2.033(5)	O21-Cu2-N5#b	93.7(6)
N7-Cu1#e	2.002(5)	N2-Cu2-N5#b	84.67(19)
		O31-Cu2-N5#b	93.6(3)
O11-Cu1-N3	87.7(2)	O31A-Cu2-N5#b	109.3(4)
O11-Cu1-N7#a	91.2(2)	Cl3-Cu2-N5#b	105.7(2)
N3-Cu1-N7#a	177.0(2)	Cl1-Cu2-N5#b	92.95(12)
O11-Cu1-N6#b	177.8(2)	Cu2-Cl1-Cu1	89.46(6)
N3-Cu1-N6#b	91.51(19)	Cu1-Cl2-Cu1#c	86.81(11)
N7#a-Cu1-N6#b	89.6(2)	N6-N5-Cu2#d	110.5(3)
O11-Cu1-Cl2	91.76(15)	C8-N5-Cu2#d	144.0(4)
N3-Cu1-Cl2	97.79(15)	N7-N6-Cu1#d	122.8(4)
N7#a-Cu1-Cl2	85.10(15)	N5-N6-Cu1#d	126.5(4)
N6#b-Cu1-Cl2	86.32(14)	N6-N7-Cu1#e	125.7(4)
O11-Cu1-Cl1	95.28(15)	N8-N7-Cu1#e	123.7(4)
N3-Cu1-Cl1	84.31(15)	C11-O11-Cu1	126.1(5)
N7#a-Cu1-Cl1	92.94(15)	C21-O21-Cu2	129.8(16)
N6#b-Cu1-Cl1	86.67(14)	C31-O31-Cu2	137.7(8)
Cl2-Cu1-Cl1	172.73(7)	C31A-O31A-Cu2	117.0(9)

Symmetry transformations used to generate equivalent atoms: equivalent atoms:

#a  $-x+1/2, y-1/4, z+1/4$ ; #b  $x-1/4, y-1/4, -z+2$ ; #c  $-x+1/4, y, -z+9/4$ ; #d  $x+1/4, y+1/4, -z+2$ ; #e  $-x+1/2, y+1/4, z-1/4$ ; #f  $-x+1/4, -y+5/4, z$

## [Cd<sub>4</sub>Cl<sub>4</sub>L(DMF)<sub>7</sub>] · DMF, 2

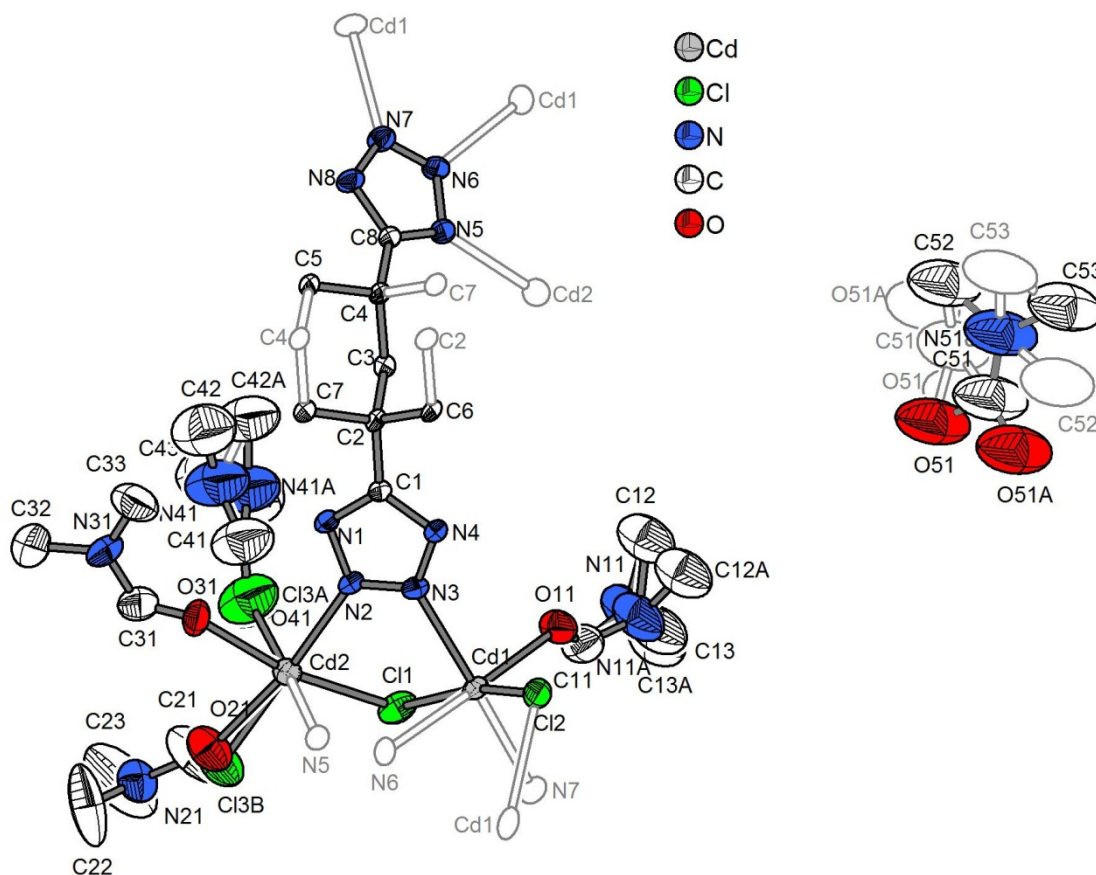


Fig. S5. ORTEP drawing of **2** at 50% probability level. The bound symmetry equivalents are shown as empty ellipsoids with dark gray outline. Two positions in the coordination sphere of Cd<sub>2</sub> is occupied by positionally disordered DMF molecules (represented by O<sub>41</sub> and O<sub>21</sub> atoms) and a chloride counteranion (represented by Cl<sub>3A</sub> and Cl<sub>3B</sub> parts). Hydrogen atoms are not shown for clarity.

The structure features positional disorder of a terminally coordinated Cl<sub>3</sub> atom and an N,N-dimethylformamide molecule. The chloride atom is disordered over two independent positions (unlike the case of the **1**, where the disorder involves only one independent position, which is shared by the anion and the DMF molecule) with populations of 0.3 (Cl<sub>3A</sub>) and 0.2 (Cl<sub>3B</sub>) with the rest represented by coordinated DMF molecules. The validity of that disorder is supported by high residual electronic density and high anisotropy of localized Cl<sub>3</sub> or O<sub>21</sub> atoms, when refined within a non-disordered model. The relative occupancy factors were estimated from an unrestrained refinement and adjusted, taking in account the demand of electroneutrality.

The coordinated DMF molecules referenced by O11 and O41 atoms feature disorder of the NMe<sub>2</sub> fragment. Partial occupancies of NMe<sub>2</sub> fragment were set to be 0.65 / 0.35 for the O11-referenced DMF molecule and 0.35/0.35 for the O41-referenced molecule (giving in total an occupancy of 0.7 for the site shared by the DMF molecule and the chloride atom). The disorder was resolved in anisotropic approximation using equality of the thermal displacement parameters (EADP) constraint for the site sharing O41 and Cl3a, as well as for O21 and Cl3b atoms. Equal anisotropic thermal parameters were assigned also to carbon atoms of the disordered methyl groups for one of the DMF molecules (C12, C12A; C13 and C13A). The C(O)-NMe<sub>2</sub> fragment was restrained to be co-planar within 0.01 Å standard deviation (FLAT). The geometry of the disordered DMF molecules was restrained using the next standard values for bond lengths: C-O 1.23(1); C(O)-N 1.31(1); N-CH<sub>3</sub> 1.47(1). A set of similarity restraints (DELU) for the thermal displacement factors of the atoms constituting the disordered DMF molecules were also applied. The H-atoms of the disordered DMF molecules were added geometrically and refined using the appropriate constraint for the idealized geometry.

There is one DMF molecule per formula unit residing in the pores of the compound. The non-coordinated guest is disordered over two overlapping positions, with the N51 nitrogen atom being common for them. Carbonyl group of this molecule adopts two orientations and, therefore, partial occupancy factors for the two contributions for the oxygen atom were set to be 0.25. This molecule was refined anisotropically, with a set of geometry (DFIX, FLAT) and thermal motion (SADI/DELU) restraints. Considering the mode of the disorder and applied restraints for thermal motion, the hydrogen atoms were not added in this case.

**Tab. S2** Bond lengths (Å) and angles (°) involving metal atoms for [Cd<sub>4</sub>Cl<sub>4</sub>L(DMF)<sub>7</sub>] · DMF, **2**.

Cd(1)-N(3)	2.292(4)	O(31)-Cd(2)-O(41)	85.4(4)
Cd(1)-O(11)	2.301(4)	N(2)-Cd(2)-O(41)	86.7(3)
Cd(1)-N(7)#a	2.316(4)	N(5)#b-Cd(2)-O(41)	174.0(3)
Cd(1)-N(6)#b	2.386(5)	O(21)-Cd(2)-Cl(3B)	11.0(6)
Cd(1)-Cl(2)	2.6120(14)	O(31)-Cd(2)-Cl(3B)	97.2(6)
Cd(1)-Cl(1)	2.6771(17)	N(2)-Cd(2)-Cl(3B)	174.7(6)
Cd(2)-O(21)	2.250(12)	N(5)#b-Cd(2)-Cl(3B)	97.7(6)
Cd(2)-O(31)	2.298(5)	O(41)-Cd(2)-Cl(3B)	88.3(7)
Cd(2)-N(2)	2.300(5)	O(21)-Cd(2)-Cl(1)	102.1(3)
Cd(2)-N(5)#b	2.416(4)	O(31)-Cd(2)-Cl(1)	168.37(13)
Cd(2)-O(41)	2.416(16)	N(2)-Cd(2)-Cl(1)	86.49(13)
Cd(2)-Cl(3B)	2.464(19)	N(5)#b-Cd(2)-Cl(1)	92.98(11)
Cd(2)-Cl(1)	2.5822(18)	O(41)-Cd(2)-Cl(1)	87.2(4)
Cd(2)-Cl(3A)	2.588(15)	Cl(3B)-Cd(2)-Cl(1)	91.5(5)
		O(21)-Cd(2)-Cl(3A)	80.2(5)
N(3)-Cd(1)-O(11)	89.28(17)	O(31)-Cd(2)-Cl(3A)	80.1(4)
N(3)-Cd(1)-N(7)#a	177.12(17)	N(2)-Cd(2)-Cl(3A)	97.5(3)
O(11)-Cd(1)-N(7)#a	90.73(17)	N(5)#b-Cd(2)-Cl(3A)	171.4(3)
N(3)-Cd(1)-N(6)#b	89.95(16)	O(41)-Cd(2)-Cl(3A)	12.6(2)
O(11)-Cd(1)-N(6)#b	176.22(19)	Cl(3B)-Cd(2)-Cl(3A)	77.7(7)
N(7)#a-Cd(1)-N(6)#b	89.86(16)	Cl(1)-Cd(2)-Cl(3A)	94.3(4)
N(3)-Cd(1)-Cl(2)	98.19(13)	Cd(2)-Cl(1)-Cd(1)	92.28(5)
O(11)-Cd(1)-Cl(2)	97.79(15)	Cd(1)#d-Cl(2)-Cd(1)	94.18(7)
N(7)#a-Cd(1)-Cl(2)	84.66(12)	N(3)-N(2)-Cd(2)	124.6(3)
N(6)#b-Cd(1)-Cl(2)	85.98(11)	N(1)-N(2)-Cd(2)	125.8(3)
N(3)-Cd(1)-Cl(1)	86.84(13)	N(2)-N(3)-Cd(1)	120.8(3)
O(11)-Cd(1)-Cl(1)	93.90(15)	N(4)-N(3)-Cd(1)	128.6(3)
N(7)#a-Cd(1)-Cl(1)	90.29(12)	C(8)-N(5)-Cd(2)#e	144.6(3)
N(6)#b-Cd(1)-Cl(1)	82.36(12)	N(6)-N(5)-Cd(2)#e	110.1(3)
Cl(2)-Cd(1)-Cl(1)	167.30(5)	N(7)-N(6)-Cd(1)#e	120.2(3)
O(21)-Cd(2)-O(31)	87.1(4)	N(5)-N(6)-Cd(1)#e	128.2(3)
O(21)-Cd(2)-N(2)	171.2(4)	N(6)-N(7)-Cd(1)#f	124.4(3)
O(31)-Cd(2)-N(2)	84.16(18)	N(8)-N(7)-Cd(1)#f	123.8(3)
O(21)-Cd(2)-N(5)#b	93.9(4)	C(11)-O(11)-Cd(1)	124.6(4)
O(31)-Cd(2)-N(5)#b	93.47(17)	C(21)-O(21)-Cd(2)	120.8(11)
N(2)-Cd(2)-N(5)#b	87.34(16)	C(31)-O(31)-Cd(2)	141.6(6)
O(21)-Cd(2)-O(41)	91.9(4)	C(41)-O(41)-Cd(2)	117.9(11)

Symmetry transformations used to generate equivalent atoms:

#a  $-x+3/2, y+1/4, z-1/4$ ; #b  $x-1/4, y+1/4, -z+1/2$ ; #c  $-x+5/4, y, -z+1/4$ ; #d  $x+1/4, y-1/4, -z+1/2$ ; #e  $-x+3/2, y-1/4, z+1/4$ ; #f  $-x+5/4, -y+1/4, z$

**[Zn<sub>3</sub>Cl<sub>2</sub>L(DMF)<sub>4</sub>] · 2DMF, **3****

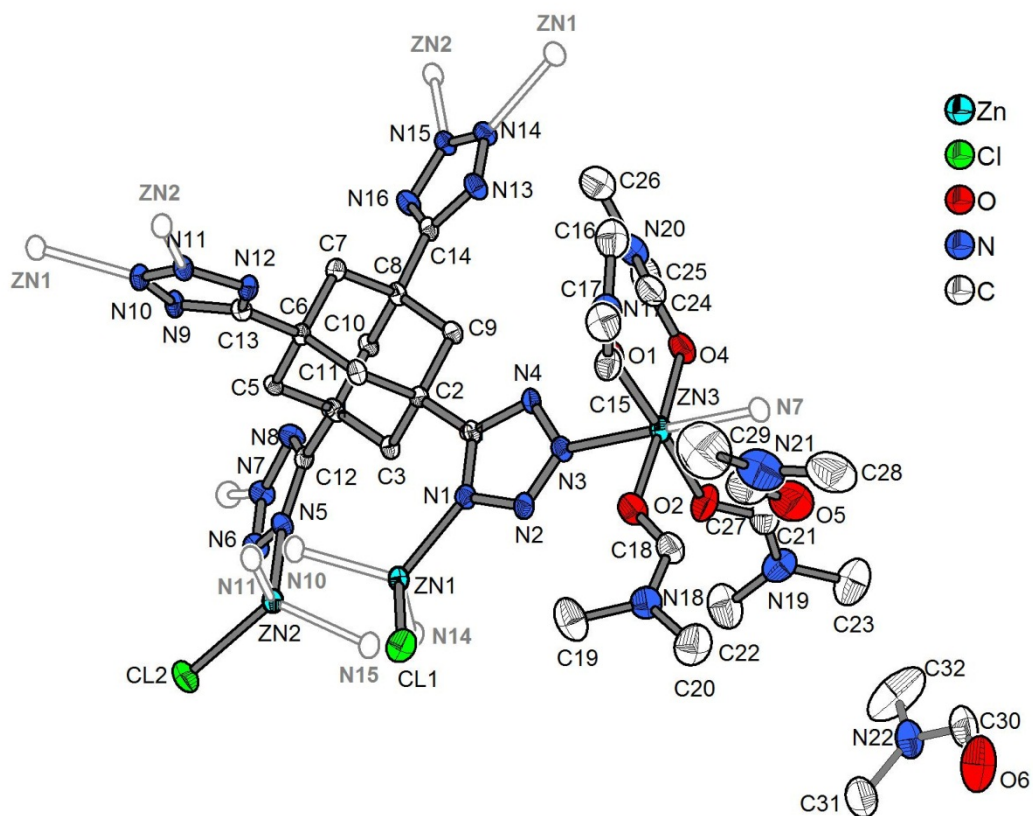


Fig. S6 ORTEP drawing of **3** at 50% probability level. The bound symmetry equivalents are shown as empty ellipsoids with dark gray outline. Hydrogen atoms are not shown for clarity.

**Tab. S3** Bond lengths (Å) and angles (°) involving the metal atoms for [Zn<sub>3</sub>Cl<sub>2</sub>L(DMF)<sub>4</sub>] · 2DMF, **3**.

Zn1-Cl1	2.1861(13)	O2-Zn3-O3	90.44(14)
Zn1-N1	2.010(4)	O2-Zn3-O4	177.04(12)
Zn1-N10#b	2.042(4)	O2-Zn3-N3	88.12(14)
Zn1-N14#c	2.046(5)	O2-Zn3-N7#e	90.91(14)
Zn2-Cl2	2.2149(15)	O3-Zn3-O4	91.45(14)
Zn2-N5	2.000(3)	O3-Zn3-N3	85.88(17)
Zn2-N11#b	2.057(4)	O3-Zn3-N7#e	94.78(17)
Zn2-N15#c	2.026(4)	O4-Zn3-N3	89.75(14)
Zn3-O1	2.101(3)	O4-Zn3-N7#e	91.20(14)
Zn3-O2	2.068(3)	N3-Zn3-N7#e	178.83(13)

Zn3-O3	2.086(4)	Zn3-O1-C15	124.3(3)
Zn3-O4	2.072(3)	Zn1#f-N14-N13	120.3(4)
Zn3-N3	2.163(5)	Zn1#f-N14-N15	130.0(3)
Zn3-N7#e	2.206(5)	N14-N15-N16	109.8(4)
		Zn2#f-N15-N14	126.5(3)
Cl1-Zn1-N1	117.89(12)	Zn3-O2-C18	130.4(3)
Cl1-Zn1-N10#b	103.65(11)	Zn3-O3-C21	136.0(5)
Cl1-Zn1-N14#c	112.82(13)	Zn3-O4-C24	120.4(3)
N1-Zn1-N10#b	113.20(15)	Zn1-N1-N2	113.3(3)
N1-Zn1-N14#c	106.00(16)	Zn1-N1-C1	141.0(3)
N10#b-Zn1-N14#c	102.34(18)	Zn3-N3-N2	125.7(3)
Cl2-Zn2-N5	114.57(10)	Zn3-N3-N4	122.5(3)
Cl2-Zn2-N11#b	104.83(12)	Zn2-N5-N6	111.2(3)
Cl2-Zn2-N15#c	114.87(14)	Zn2-N5-C12	141.8(3)
N5-Zn2-N11#b	111.28(15)	Zn3#d-N7-N6	124.3(4)
N5-Zn2-N15#c	107.50(14)	Zn3#d-N7-N8	124.3(3)
N11#b-Zn2-N15#c	103.20(18)	Zn1#b-N10-N9	121.5(4)
O1-Zn3-O2	88.74(12)	Zn1#b-N10-N11	128.0(3)
O1-Zn3-O3	177.69(15)	N10-N11-N12	109.9(4)
O1-Zn3-O4	89.29(12)	Zn2#b-N11-N10	128.2(3)
O1-Zn3-N3	91.93(15)	Zn2#b-N11-N12	121.9(4)
O1-Zn3-N7#e	87.40(14)	Zn2#f-N15-N16	123.6(4)

#a = 3/2-x, 1/2+y, 5/2-z; #b = 1-x, -y, 2-z; #c = -1/2+x, 1/2-y, -1/2+z; #d = -1/2+x, 1/2-y, 1/2+z; #e = 1/2+x, 1/2-y, -1/2+z; #f = 1/2+x, 1/2-y, 1/2+z



**Fig. S7** Platelet crystals of **4** in mother solution in polarized light.

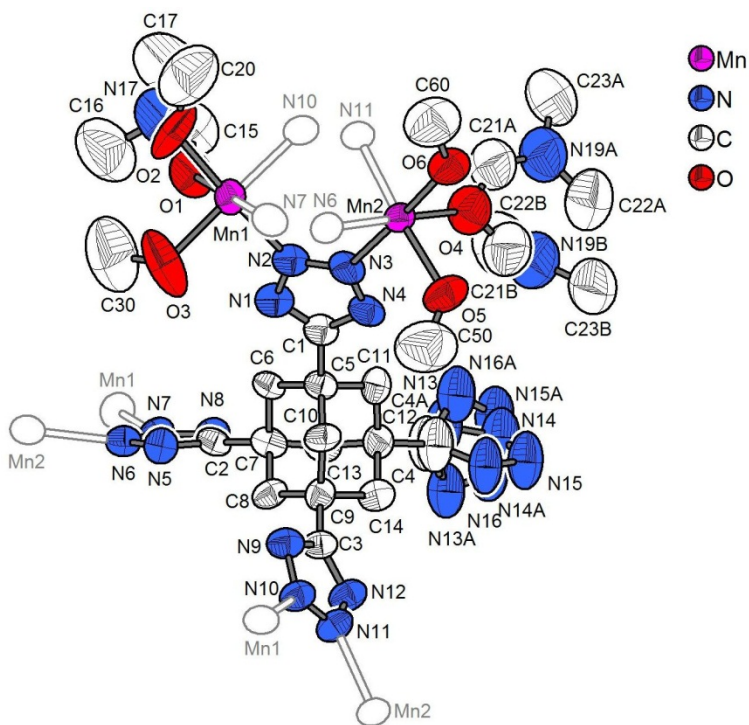


**Fig. S8.** ORTEP drawing of **4** at 50% probability level. The bound symmetry equivalents are shown as empty ellipsoids with dark gray outline. Hydrogen atoms are not shown for clarity.

The structure of **4** features a number of crystallographic problems due to low crystallinity caused by progressing structural collapse after isolation from the mother liquor and hence by low quality of the diffraction experiments.

The non-coordinated tetrazolate group of the adamantane ligand is disordered in a way that the two equal contributors adopt a nearly orthogonal orientation. The disorder was modelled with a set of soft restraints (DFIX) for the standard ring geometry (i.e. C-N = 1.365 Å; N1-N2 and N3-N4 = 1.320 Å; N2-N3 = 1.332 Å) and keeping the ring atoms coplanar within 0.01 Å (FLAT). Similarity restraints (SIMU) were also applied for the thermal motion of all ring atoms constituting two components of the disorder, refined with different PART numbers.

Atoms of the initially refined coordinated DMF and methanol ligands had large thermal displacement parameters having suggested a probable disorder. In one case a disorder of a coordinated DMF ligand (at Mn2 ion) was successfully resolved. The refined scheme considers common O-atom (coordinated to Mn2) and two CH-NMe<sub>2</sub> fragments with 0.5 population, which were refined in different PARTs. Attempts to resolve possible disorder for the second coordinated DMF (at Mn1) and four methanol ligands had not afford a stable model and the subsequent refinement have led to divergence. In order to improve the refinement stability, both DMF molecules were refined with restrained (DFIX) standard geometry using the next bond length values: C-O = 1.230(10) Å C(O)-N = 1.310(10) Å; N-C(Me) 1.470(10) Å and FLAT 0.01 restraints for the planarity of C(O)-NMe<sub>2</sub> fragment. As well, similarity restraints (SIMU, DELU) were used for the anisotropic thermal parameters.

In the case of coordinated methanol ligands, the C-O bond lengths were restrained at 1.42(2) Å, and similarity restraints for anisotropic thermal values were used separately for every oxygen and corresponding carbon atoms. The hydrogen atoms were added geometrically inheriting the 0.5 occupancy factors for the disordered DMF molecule. OH-hydrogens of the coordinated methanol molecules were not added. We note that for two of the methanol ligands the positions of OH-hydrogens are evident from the analysis of intermolecular O...N separations suggesting convenient OH...N hydrogen bonding between these MeOH molecules and non-coordinated tetrazolate groups (0.5+x, -y, z) (O...N = 2.62-2.84 Å).

Solvate DMF and methanol molecules, which populate voids of the framework (total solvent accessible area is 1731 Å<sup>3</sup> per unit cell) are badly disordered. We were not successful in the refinement of the disorder in the solvent region of the structure. Therefore, this disordered residual electron density was modelled using SQUEEZE routine as it is implemented in PLATON. Four voids of 436-437 Å were found (474 e/cell) corresponding to

1 DMF, 2 MeOH and 2 H<sub>2</sub>O guest molecules per formula unit, as explained in the next section.

*Estimation of the solvent content based on the structural data*

- The molecular volumes of the coordinated and uncoordinated solvent molecules were estimated using (SOLV, Platon) procedure: values of 90.4 Å<sup>3</sup> (DMF) and 36.75 Å<sup>3</sup> (MeOH) were found for the coordinated molecules (the values were used for cross-checking the residual volume obtained directly by SQUEEZE, Platon). The molecular volumes of the non-coordinated solvent molecules 127 Å<sup>3</sup> (DMF), 67 Å<sup>3</sup> (MeOH) were calculated from the densities of the solvents in the liquid state, while the ~ 40 Å<sup>3</sup> value for H<sub>2</sub>O was used as given in output for SOLV (Platon).

- 437 Å<sup>3</sup> residual volume (found by SQUEEZE) corresponds to 1 DMF, 2 MeOH and 2 H<sub>2</sub>O non-coordinated guest molecules (341 Å<sup>3</sup>) with a packing factor of 0.78.

Note: the packing factor doesn't relate directly with the usually implied packing index. Formally, the molecular volume calculated using the density of the corresponding liquid is implicitly assumes the classic packing index. Though, it is clear that the solvent molecules cannot precisely fill the cavities and the real packing factor normally should be less than 1.

The presence of water in the pores is quite probable as its presence allows better packing possibilities. On the other hand, there is only a small amount of water in the synthetic medium, introduced only by the hydrated ligand, so the amount of water could be somewhat overestimated. The current value is a compromise with the elemental analysis data, which necessarily assumes the presence of water (otherwise the carbon content tends to be too high).

*Solvent content estimation based on the electronic count* (by SQUEEZE procedure, Platon): An unexpectedly low value of ~175 e per formula unit was found for a structure stripped of all solvent molecules, coordinated and non-coordinated as well. DMF(40 e), MeOH(18 e), H<sub>2</sub>O (10 e) shows that the limit is almost reached at accounting the coordinated 2 DMF + 4 MeOH molecules with the total of 152 e. Thus, the determination of solvent content based on electron count is not reliable and the estimation based on solvent accessible volumes was preferred.

**Tab. S4** Bond lengths (Å) and angles (°) involving metal atoms for [Mn<sub>2</sub>L(DMF)<sub>2</sub>(MeOH)<sub>4</sub>] DMF · 2MeOH · 2H<sub>2</sub>O, **4**

Mn1-N2	2.2525	O4-Mn2-N6#b	178.62
Mn2-N3	2.2394	O6-Mn2-N6#b	91.3918
Mn2-N6#b	2.2305	O5-Mn2-N6#b	93.42
Mn1-N7#b	2.2674	O4-Mn2-N3	90.92
Mn1-N10#a	2.2485	O6-Mn2-N3	177.72
Mn2-N11#a	2.2515	O5-Mn2-N3	94.5119
Mn1-O1	2.1834	N6#b-Mn2-N3	88.0017
Mn1-O2	2.1616	O4-Mn2-N11#a	92.12
Mn1-O3	2.1596	O6-Mn2-N11#a	89.0718
Mn2-O4	2.1356	O5-Mn2-N11#a	176.22
Mn2-O5	2.1764	N6#b-Mn2-N11#a	88.7518
Mn2-O6	2.1744	N3-Mn2-N11#a	88.7118
		N3-N2-Mn1	126.43
O3-Mn1-O2	91.33	N1-N2-Mn1	125.14
O3-Mn1-O1	89.82	N4-N3-Mn2	124.24
O2-Mn1-O1	86.72	N2-N3-Mn2	126.33
O3-Mn1-N10#a	178.13	N7-N6-Mn2#c	130.43
O2-Mn1-N10#a	90.23	N5-N6-Mn2#c	122.23
O1-Mn1-N10#a	91.5419	N8-N7-Mn1#c	125.13
O3-Mn1-N2	91.83	N6-N7-Mn1#c	122.33
O2-Mn1-N2	175.82	N11-N10-Mn1#d	128.63
O1-Mn1-N2	90.62	N9-N10-Mn1#d	121.64
N10#a-Mn1-N2	86.8117	N12-N11-Mn2#d	125.34
O3-Mn1-N7#b	90.32	N10-N11-Mn2#d	123.94
O2-Mn1-N7#b	92.52	C15-O1-Mn1	131.35
O1-Mn1-N7#b	179.12	C20-O2-Mn1	129.68
N10#a-Mn1-N7#b	88.3717	C30-O3-Mn1	115.610
N2-Mn1-N7#b	90.2616	C21A-O4-Mn2	124.48
O4-Mn2-O6	89.72	C21B-O4-Mn2	120.89
O4-Mn2-O5	85.82	C50-O5-Mn2	130.08
O6-Mn2-O5	87.7318	C60-O6-Mn2	132.96

#a -x+1/2,y,z-1/2; #b x+1/2,-y+1,z; #c x-1/2,-y+1,z; #d -x+1/2,y,z+1/2.

## TGA

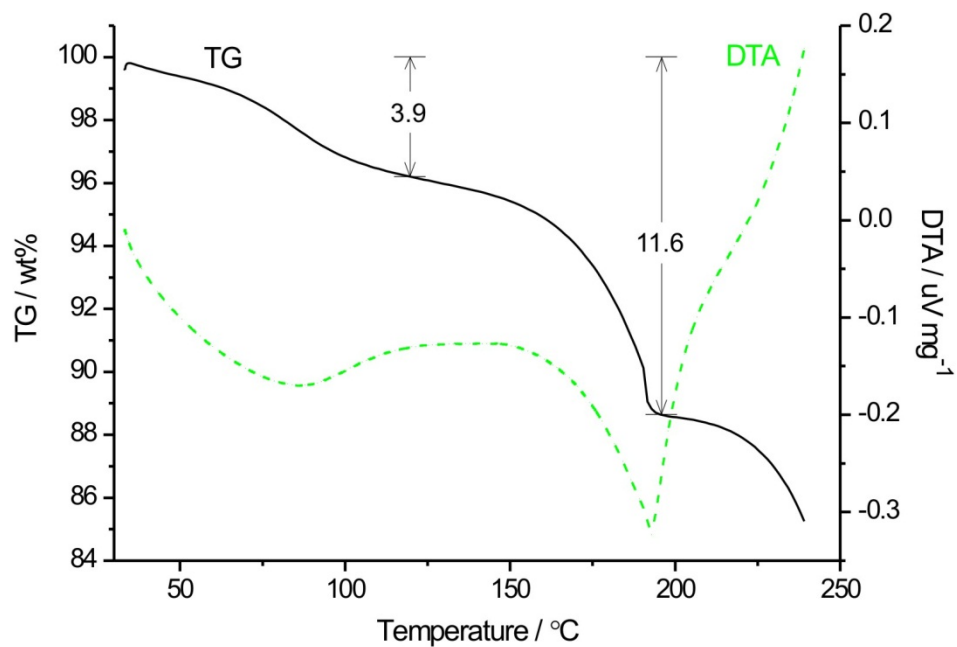


**Fig. S9.** Thermogravimetric analysis (TGA) and differential scanning calorimetry plots of the ligand hydrate,  $\text{H}_4\text{L} \cdot 3\text{H}_2\text{O}$ . The data was collected by Netzsch STA 449 C Jupiter instrument. The ligand decomposition accelerates after  $\sim 220^\circ\text{C}$  and near-explosive decomposition were observed around  $250^\circ\text{C}$  on bulk sample, which limited the range of the measurement.

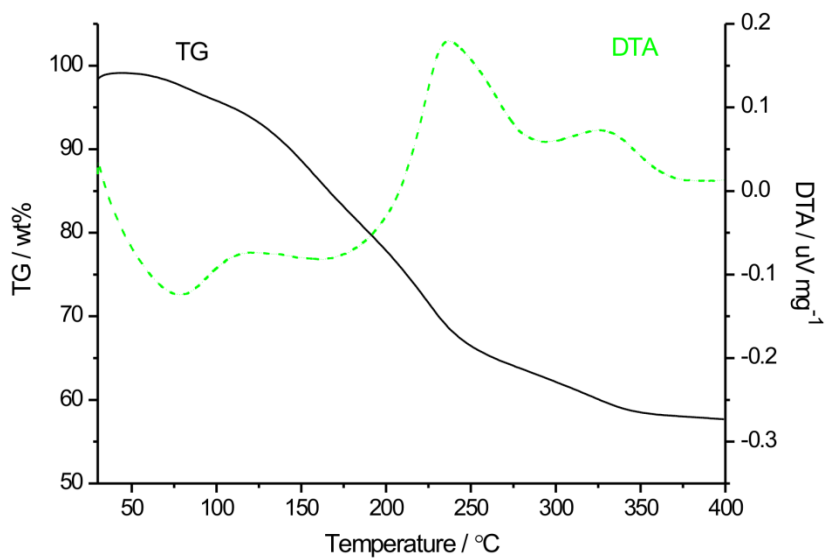


**Fig. S10.** Thermogravimetric analysis and differential scanning calorimetry of the  $[\text{Cu}_4\text{Cl}_4\text{L}(\text{DMF})_5] \cdot \text{DMF}$ , **1** compound. The data were collected by Netzsch STA 449 C Jupiter instrument. Note that the exothermic decomposition of the ligand starting slightly below  $200^\circ\text{C}$ .

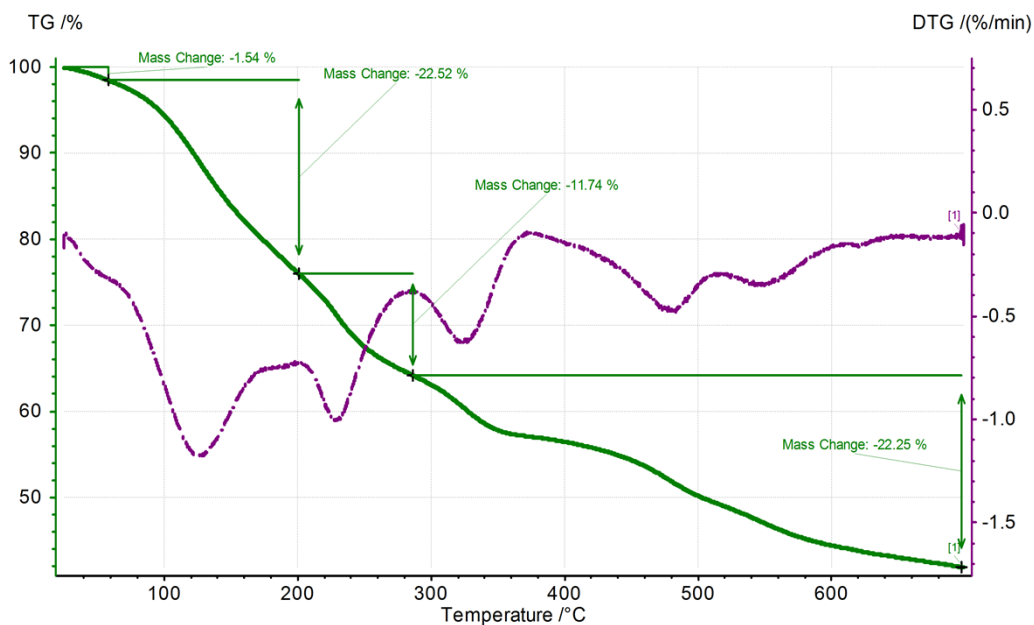


**Fig. S11.** Thermogravimetric analysis of  $[\text{Cu}_4\text{Cl}_4\text{L}(\text{DMF})_5] \cdot \text{DMF}$ , **1** compound collected until complete decomposition of the ligand. The data was collected by Netzsch TG 209 F3 Tarsus instrument. The imprecisely defined interval of DMF weigh loss at 24.1 - 35.8% corresponds to  $\sim 3.5 - 6.1$  solvent molecules (starting from  $\sim 210^\circ\text{C}$  the weight loss associated with the decomposition of the ligand also contributes to the balance).

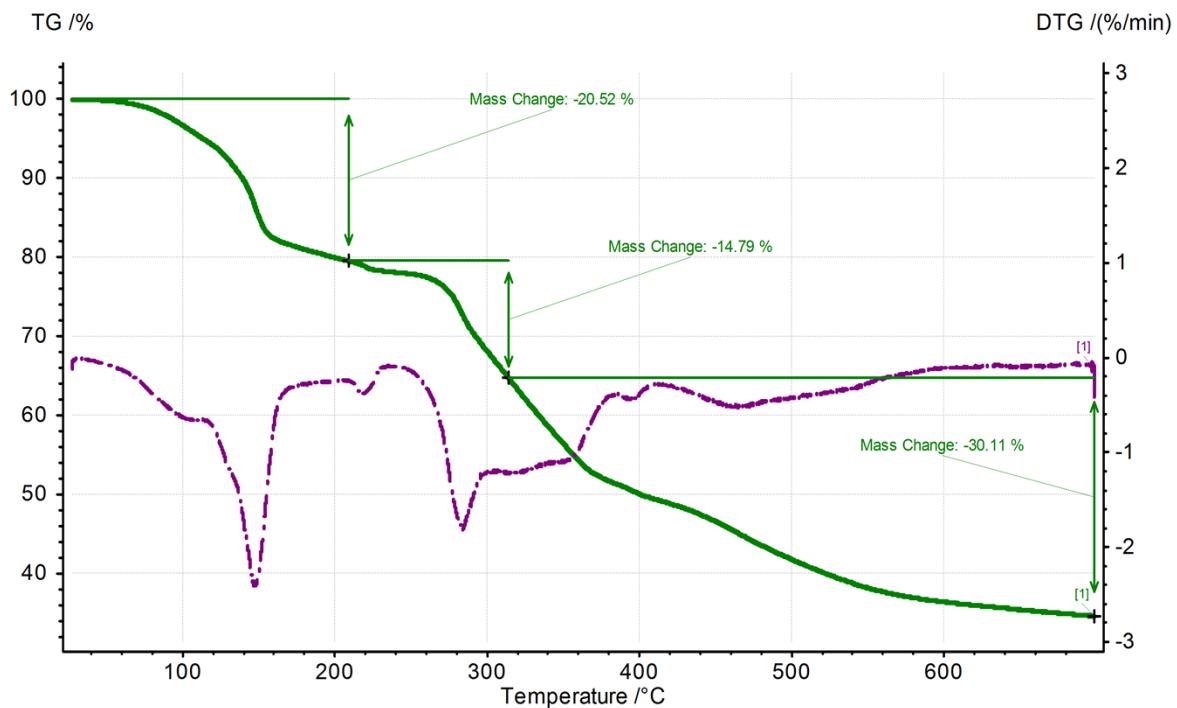


**Fig. S12.** Thermogravimetric analysis of  $[\text{Cd}_4\text{Cl}_4\text{L}(\text{DMF})_7] \cdot \text{DMF}$ , **2**. The data was collected by Netzsch TG 209 F3 Tarsus instrument. The imprecisely defined interval of DMF weight loss at 20.52 – 35.31% corresponds to 3.5 – 7.4 molecules of solvent (starting from  $\sim 210^{\circ}\text{C}$  the weight loss associated with the decomposition of the ligand also contributes to the balance)

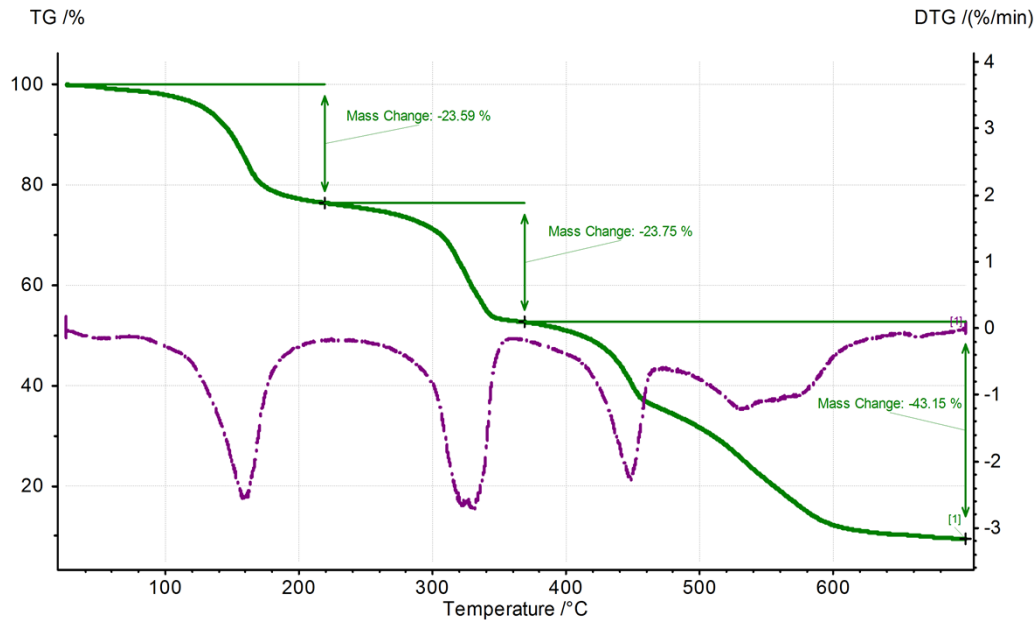


**Fig. S13.** Thermogravimetric analysis of  $[\text{Zn}_3\text{Cl}_2\text{L}(\text{DMF})_4] \cdot 2\text{DMF}$ , **3**. The data was collected by Netzsch TG 209 F3 Tarsus instrument. The imprecisely defined interval of DMF weight loss at 23.59 – 47.34% corresponds to 2.83-8.26 DMF molecules (the decomposition of the ligand on the second wave, starting at app 210°C also contributes to the balance). The two stage weight loss is consistent with two non-coordinated DMF molecules and four coordinated DMF molecules witnessed by the single crystal XRD structure.

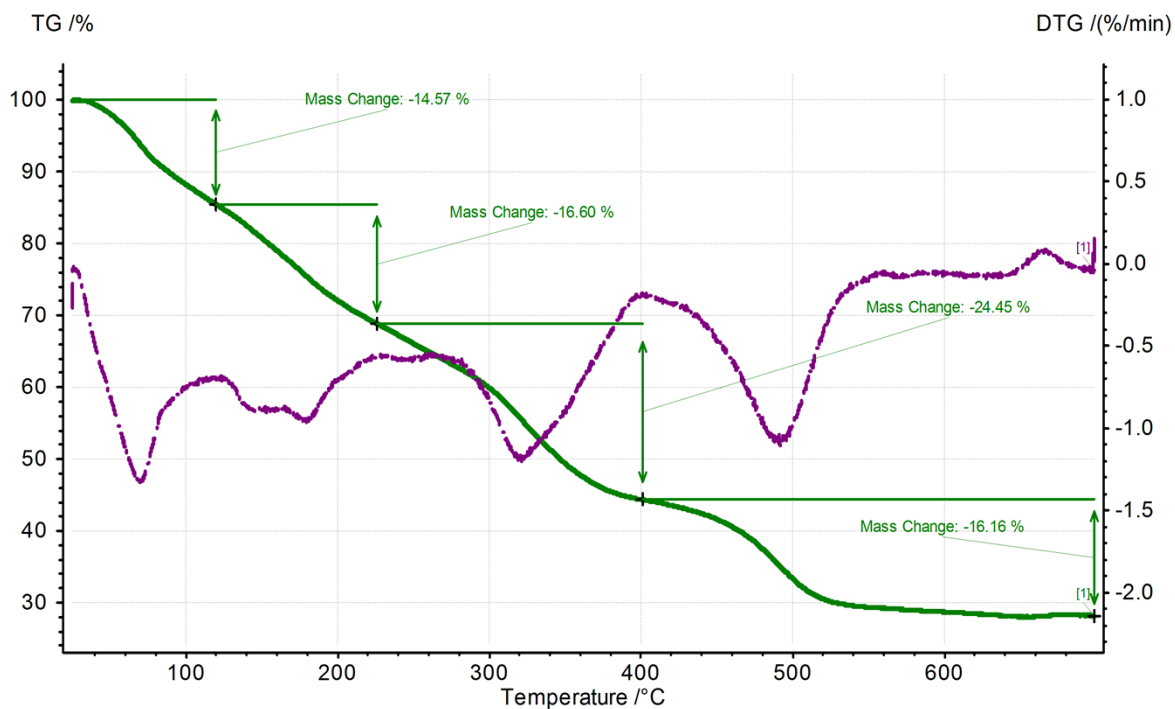


**Fig. S14.** Thermogravimetric analysis of  $[\text{Mn}_2\text{L}(\text{DMF})_2(\text{MeOH})_4] \cdot \text{DMF} \cdot 2\text{MeOH} \cdot 2\text{H}_2\text{O}$ , **4**. The data was collected by Netzsch TG 209 F3 Tarsus instrument. The non-differentiated weight loss did not allow the precise determination of the solvent content. The interval of 31.1-55.7% weight loss associated with the solvents corresponds to 230-646 interval of molecular weight per formula unit. The proposed composition with total molecular weight of solvents at 447.6 is a compromise between available solvent accessible volume in the XRD structure and the elemental analysis data.

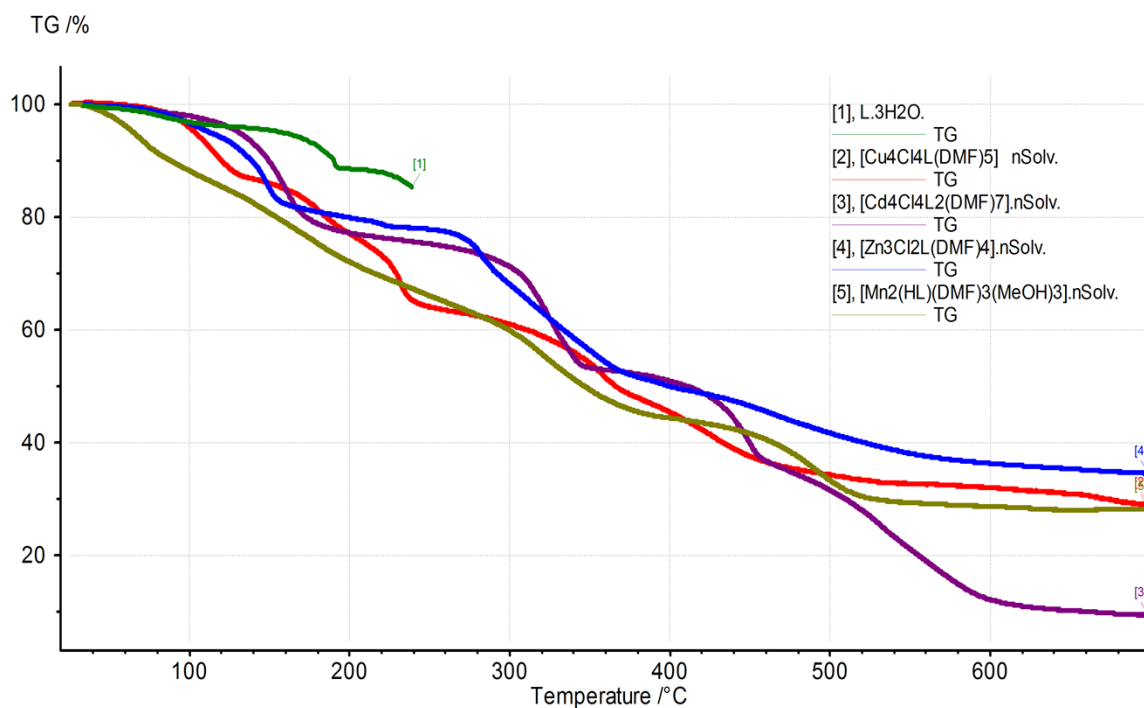


**Fig. S15.** Comparative TGA of the ligand hydrate and the as-synthesized compounds. The ligand decomposes near-explosively around 250°C, which explains the used range of the measurement.

## IR spectroscopy

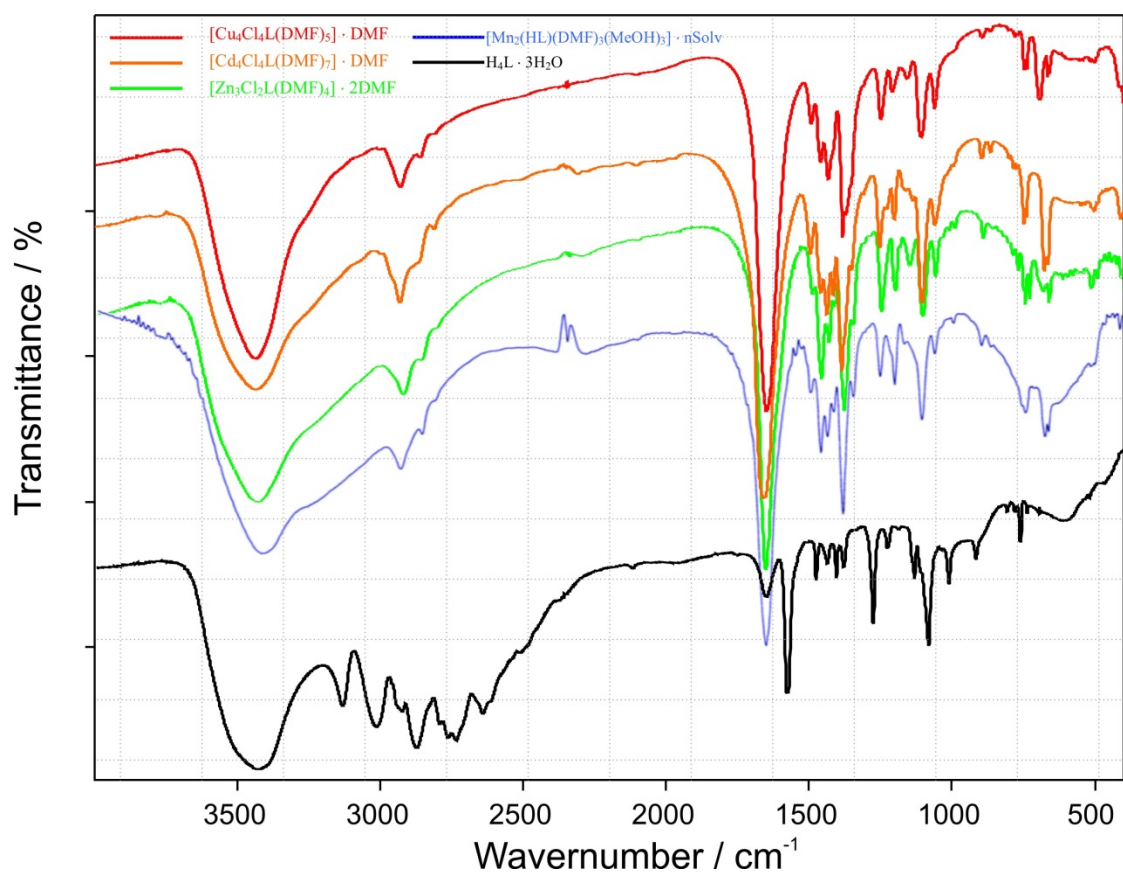


**Fig. S16.** IR spectra of the compounds **1** (red), **2** (orange), **3** (green), **4** (blue) and  $\text{H}_4\text{L} \cdot 3\text{H}_2\text{O}$  (black). Note the characteristic CO(DMF) band at 1650-1660  $\text{cm}^{-1}$  for the coordination compounds.

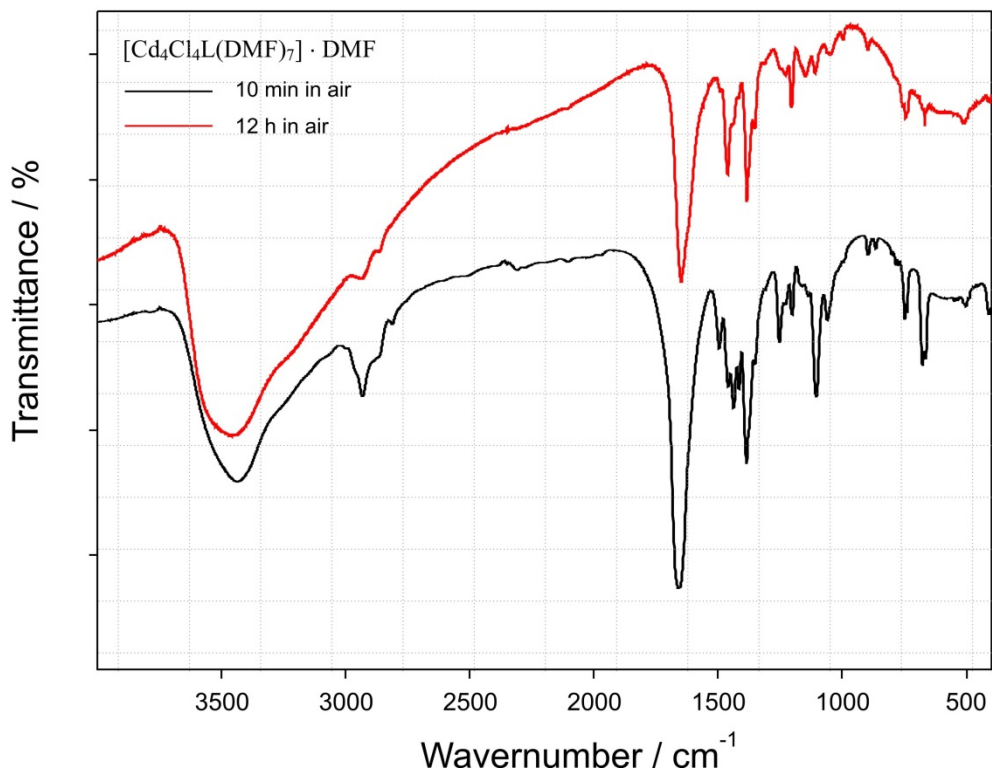


Fig. S17. IR stability test of **2** in air. Note the loss of DMF ( $\sim 1650 \text{ cm}^{-1}$ ).

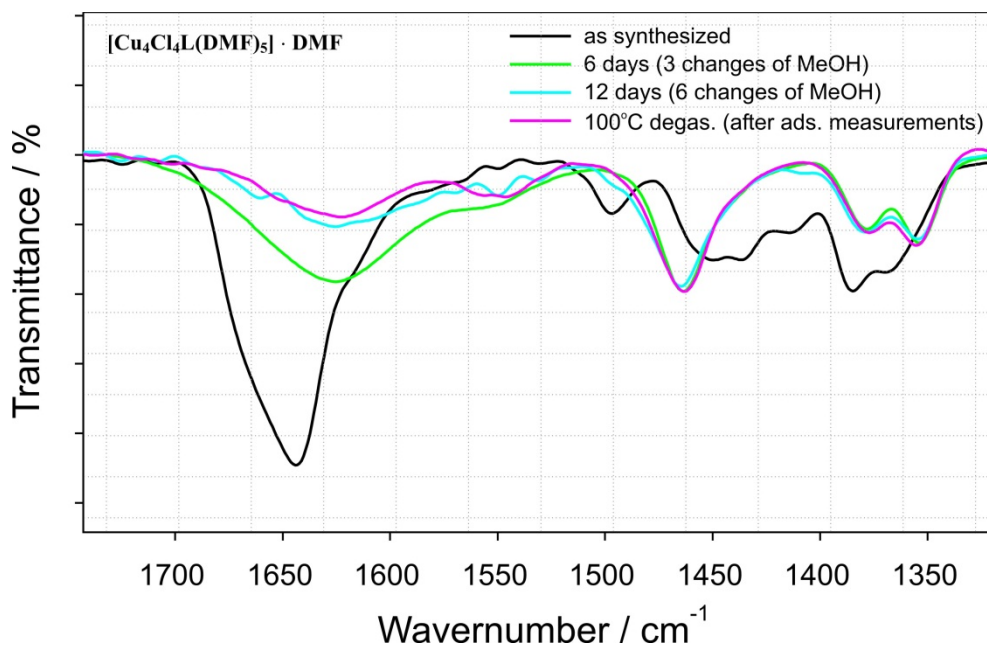
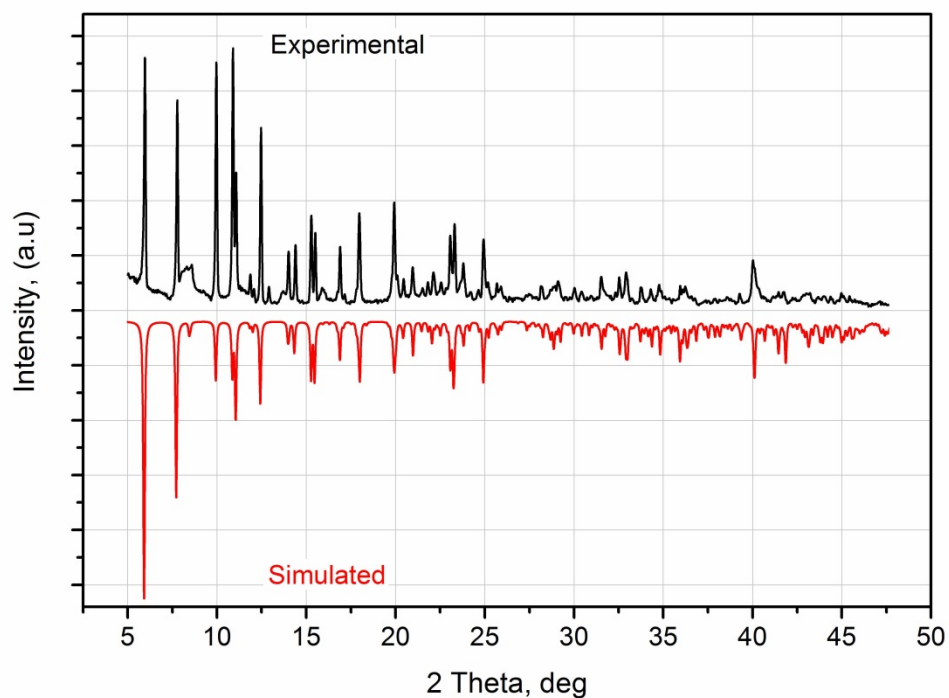
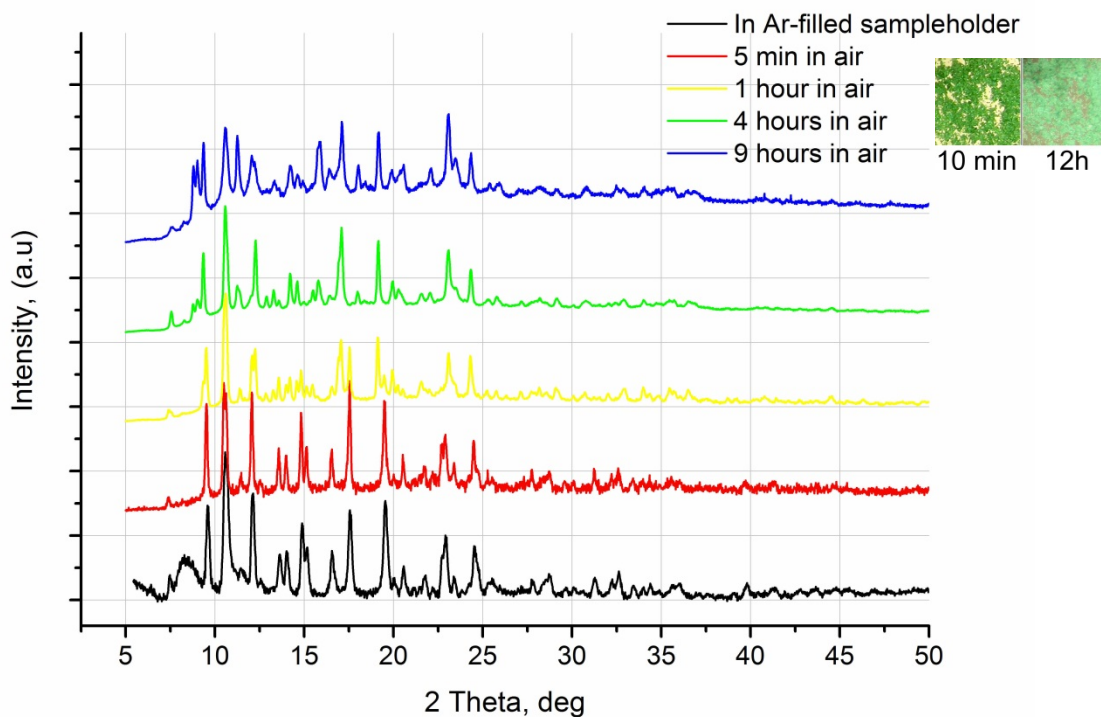


Fig. S18. IR monitoring of the solvent exchange at room temperature in **1**. Note the almost complete disappearance of DMF after 12 days of soaking.

## Powder XRD measurements



**Fig. S19.** Comparison of the experimental and simulated PXRD patterns for  $[\text{Cu}_4\text{Cl}_4\text{L}(\text{DMF})_5] \cdot \text{DMF}$ , **1**. The quality measurement was performed using a Bruker D8 diffractometer on a sample packed while fresh in a capillary.



**Fig. S20.** Stability test for  $[\text{Cu}_4\text{Cl}_4\text{L}(\text{DMF})_5] \cdot \text{DMF}$ , **1** in air. The measurements were done on a low-background Si sampleholder using a Bruker D2 instrument and the data are given uncorrected (background, small uncompensated angular shift associated with the thickness of the sample), except the set corresponding to the special 'dome' sampleholder filled with Ar, in the case of which the background is subtracted (a broad peak at  $2\theta \sim 7^\circ$  is partially an artifact of the measurement and the intensities below  $2\theta \sim 8^\circ$  are strongly down-weighted in all cases due to peculiarities of the experimental setup). Significant change of the pattern takes place after tenth of minutes in air.

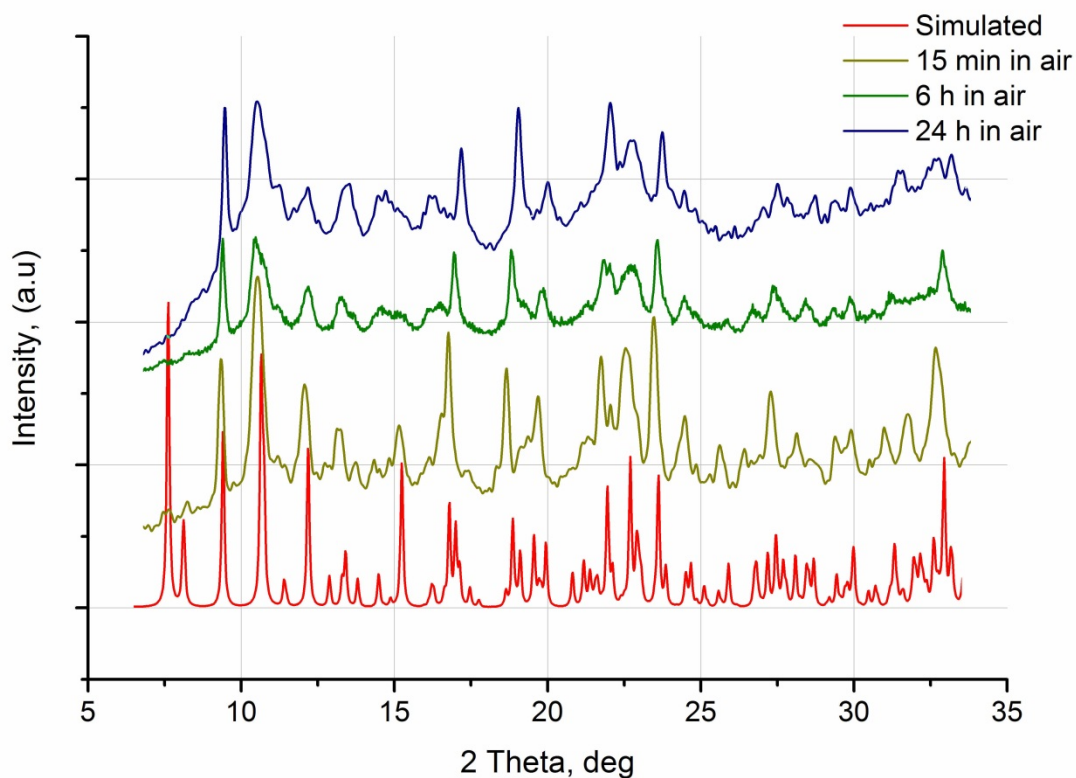


**Fig. S21.** Comparison of the experimental and simulated PXRD patterns for  $[\text{Cd}_4\text{Cl}_4\text{L}(\text{DMF})_7] \cdot \text{DMF}$ , **2** as well as results of stability tests in air. The measurement is done using a low-background Si sample holder on a Bruker D2 instrument. The measurement results are uncorrected against angular shift caused by non-zero sample thickness. Background subtraction and smoothing were applied for the short measurement at  $\sim 15$  min in air. The intensities below  $2\theta \sim 8^\circ$  are strongly down-weighted in all cases due to peculiarities of the experimental setup).

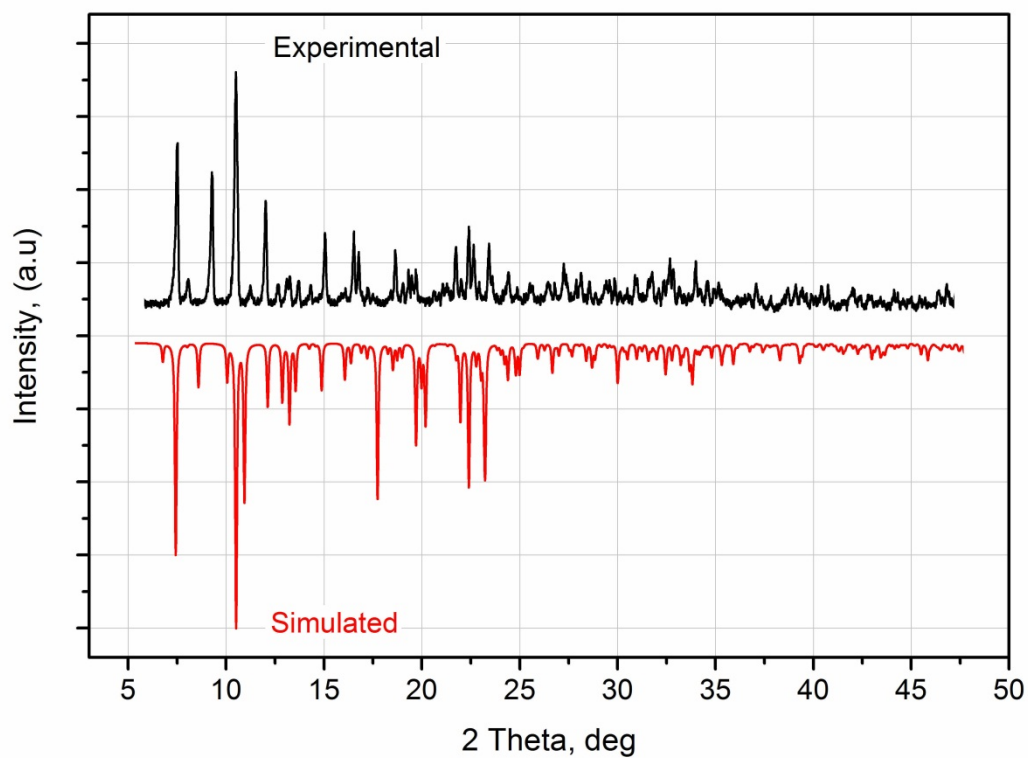


**Fig. S22.** Comparison of the experimental and simulated PXRD patterns for  $[\text{Zn}_3\text{Cl}_2\text{L}(\text{DMF})_4] \cdot 2\text{DMF}$ , **3**. The quality measurement was performed using a Bruker D8 diffractometer on a sample packed in a capillary .

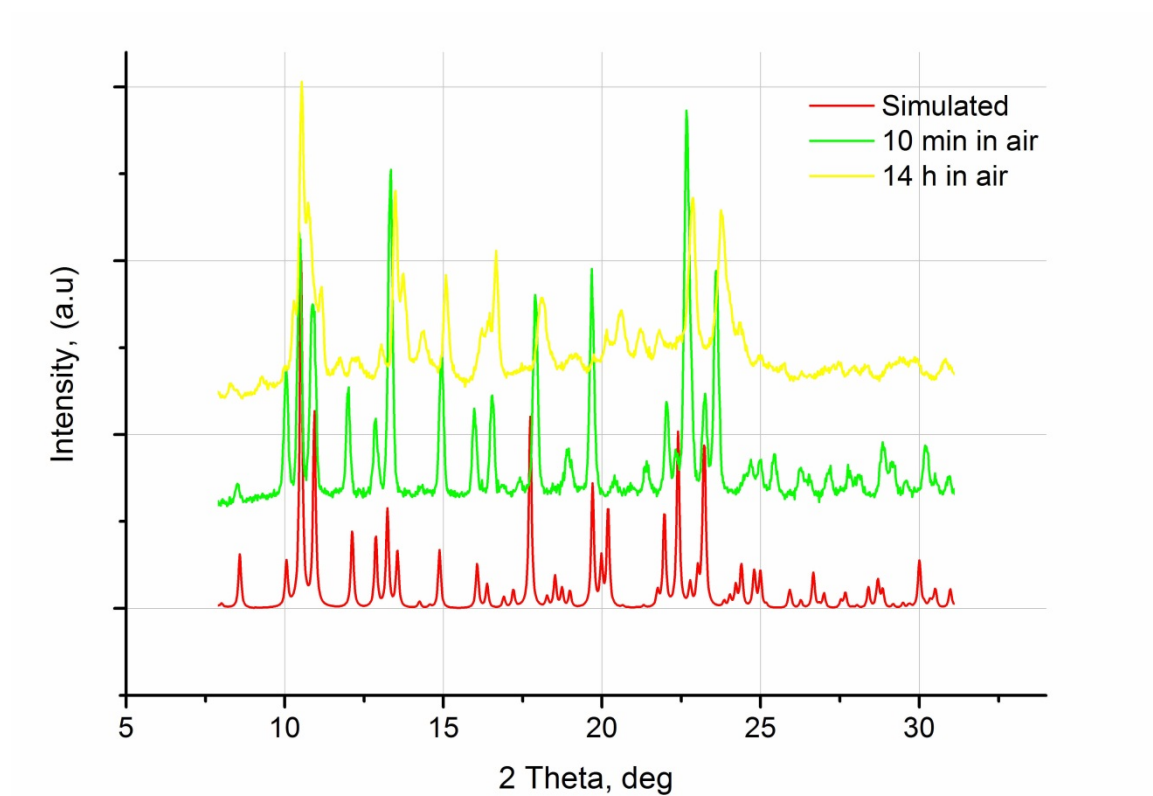


**Fig. S23.** Stability test for  $[\text{Zn}_3\text{Cl}_2\text{L}(\text{DMF})_4] \cdot 2\text{DMF}$ , **3** in air. The measurements were done on a low-background Si sampleholder using a Bruker D2 instrument and the data are given uncorrected (background, small uncompensated angular shift associated with the thickness of the sample). The intensities below  $2\theta \sim 8^\circ$  are strongly down-weighted in all cases due to peculiarities of the experimental setup). Significant deterioration takes place within hours in air.

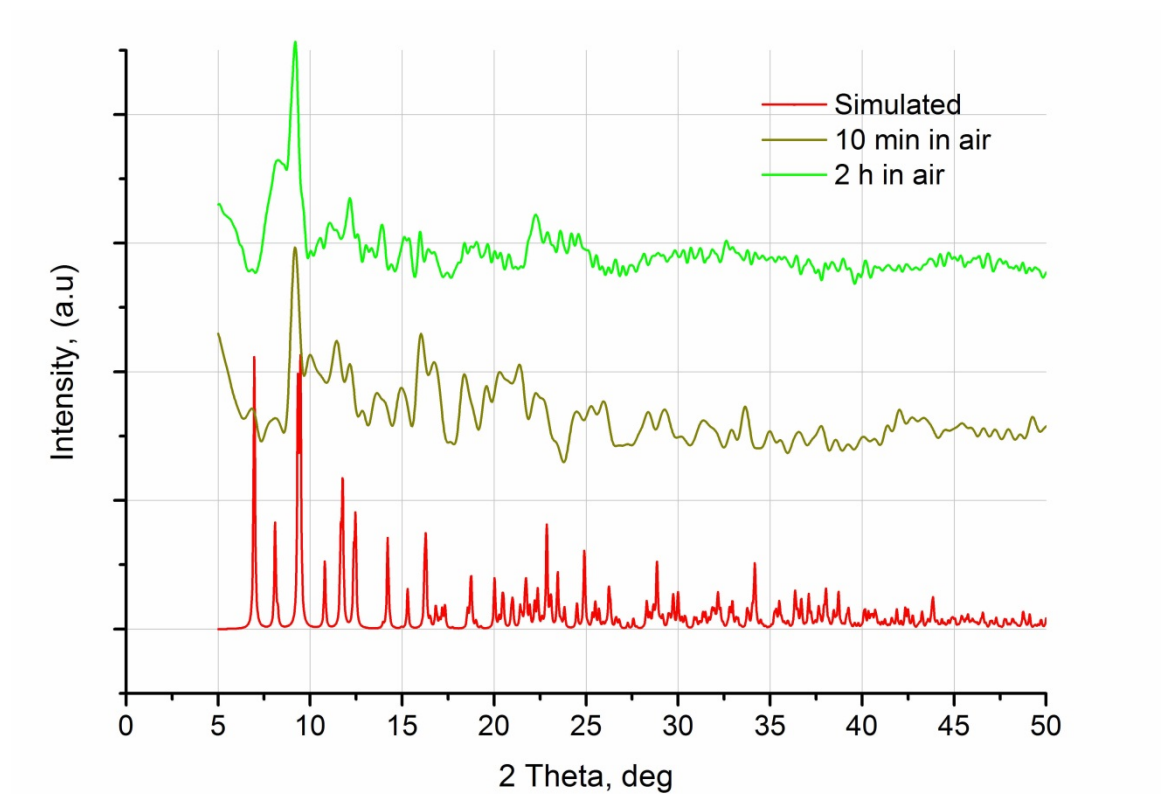


**Fig. S24.** Comparison of the experimental and simulated PXRD patterns for  $[\text{Mn}_2\text{L}(\text{DMF})_2(\text{MeOH})_4] \text{DMF} \cdot 2\text{MeOH} \cdot 2\text{H}_2\text{O}$ , **4** as well as results of stability tests in air. The measurement is done using a low-background Si sample holder on a Bruker D2 instrument. The measurement results are uncorrected against angular shift caused by non-zero sample thickness. Background subtraction and smoothing were applied for all experimental data. The intensities below  $2\theta \sim 8^\circ$  are strongly down-weighted in all cases due to peculiarities of the experimental setup). The sample is not stable against loss of solvent even during short time.

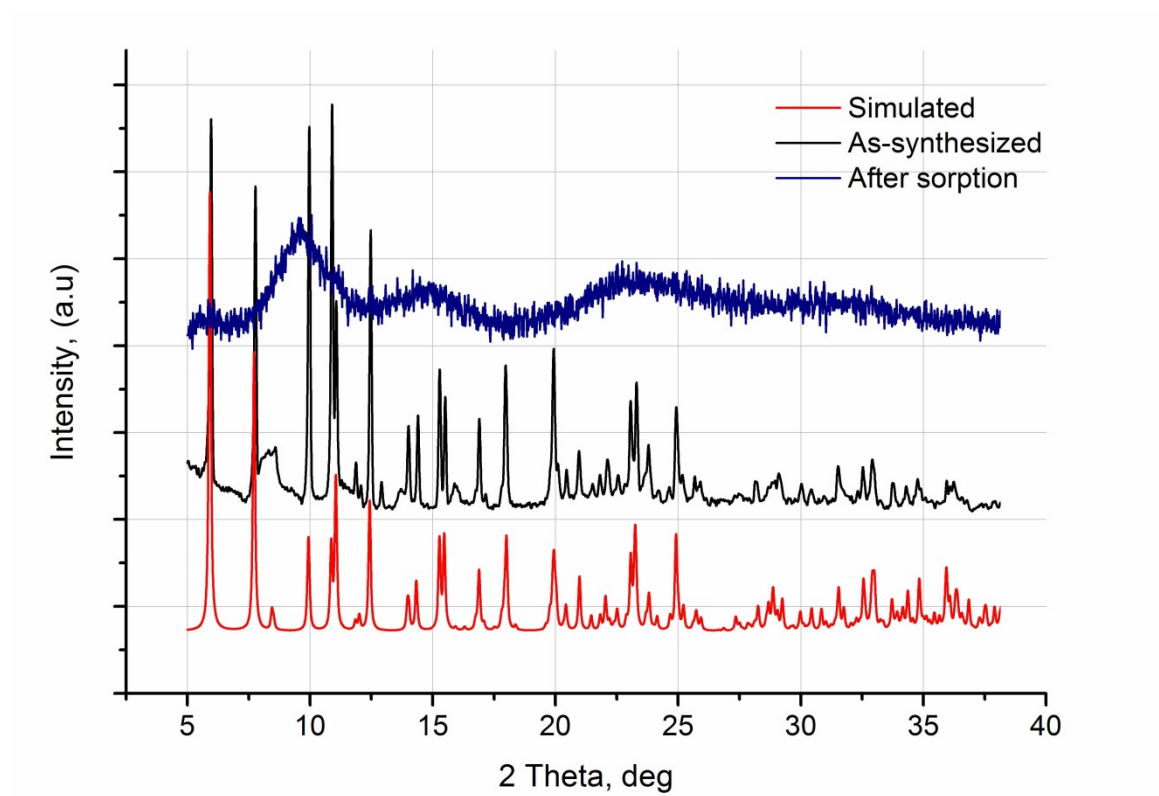


**Fig. S25.** Comparison of the PXR D pattern for the sample after activation and sorption measurements with as-synthesized sample and the simulated pattern for  $[\text{Cu}_4\text{Cl}_4\text{L}(\text{DMF})_5] \cdot \text{DMF}$ , **1**. Practically complete loss of crystallinity is observed.

## ***Sorption studies***

Sorption isotherms were measured using Quantachrome iQ and Micromeritics ASAP2020 automatic gas sorption analyzers equipped with oil-free vacuum pumps (ultimate vacuum  $<10^{-8}$  mbar) and valves, which guaranteed contamination free measurements. The solvent exchange was done as follows: approx. 50mg of sample freshly filtered from the mother liquor was soaked in ~6 ml of dry methanol for 5+ days (as indicated in the text) in a closed vial at room temperature. The supernatant solvent was regularly exchanged once per 5 days for long soaking times. The supernatant was removed in inert atmosphere just prior the experiment, the sample was pre-dried in 10 Torr vacuum and RT and transferred in a nitrogen filled and pre-weighed sample tube capped with a septum, and the tube was immediately purged to maintain the strictly inert conditions and weighted. The samples were degassed under vacuum ultimate vacuum using conditions specified below (in a typical experiment a pre-treatment at 30°C for a few hours was followed by heating at 0.5-2°C/min to final temperature and degassed for 12-24h). The weight of the degassed sample was determined by a repeated weighting of the sample tube. Ultra high purity (UHP, grade 5.0, 99.999%) nitrogen and helium gases were used for the measurements; the latter was used for performing for the determination of the cold and warm free space.

Tab. S5 Volume (STP) of N<sub>2</sub> and H<sub>2</sub> gases adsorbed at 1 bar pressure and 77K. The samples were exchanged with MeOH and degassed at the indicated temperatures (given in brackets). The data for **2-4**, in some cases extrapolated, is indicative only and serve as an account for nearly non-existent microporosity (such low uptakes measured for ~30-60 mg sample weights have large experimental errors, which could easily reach 10%).

Compound	V <sub>H2</sub> , cm <sup>3</sup> / g (T <sub>deg</sub> , °C)	V <sub>N2</sub> , cm <sup>3</sup> / g (T <sub>deg</sub> , °C) at P/P <sub>0</sub> = 0.95
[Cu <sub>4</sub> Cl <sub>4</sub> L(DMF) <sub>5</sub> ] · DMF, <b>1</b>	87.6 (70) 79.8 (70)* 85.4 (70)* 89.5(80)**	281 (30) 251 (80)**
[Cd <sub>4</sub> Cl <sub>4</sub> L(DMF) <sub>7</sub> ] · DMF, <b>2</b>	1.1 (30) 7.4 (70) 7.5 (120)	8.6 (30)
[Zn <sub>3</sub> Cl <sub>2</sub> L(DMF) <sub>4</sub> ] · 2DMF, <b>3</b>	5.8 (30) 23.3 (70) 19.5 (120)	34.8 (30)
[Mn <sub>2</sub> L(DMF) <sub>2</sub> (MeOH) <sub>4</sub> ] DMF · 2MeOH · 2H <sub>2</sub> O, <b>4</b>	16.9 (30)	19.5 (30)

\* - Repeated measurements

\*\* - An independent checking measurement, performed on a freshly prepared sample using a Micromeritics ASAP 2020 instrument.

Indirect different evidences based on the structural and TGA data suggest that the compounds **1-4** are not thermally robust, with a possible exception of the cadmium compound **2**. According to the TGA the decomposition of the ligand in the complexes starts at app. 200-210°, which sets a natural limit to the degassing temperature. The copper compound **1**, containing DMF is expected to be unstable towards reduction of copper at a temperatures exceeding 80°C, which was indeed observed (the colour of the compound degassed at 120°C turns to deep brown with a reddish tint). The zinc compound **3** is expected to collapse easily as the degassed structure should contain zinc atoms with a coordination number of 2 in the vicinity of tetrazolate groups possessing an excess of donor groups. The cadmium compound **2** is anticipated to be the most stable, but due to the small size of the pores the escape of DMF at high temperatures might damage the structure as well.

With the given prerequisites the solvent exchange approach for sample preparation was attempted for all the compounds. 40-60 mg samples were soaked in a large excess of

MeOH (~5 ml; spectrophotometric grade, Aldrich). The exchange in hermetically closed vials was allowed to proceed for at least 5 days at room temperature with at least two exchanges of MeOH (in the case of **1** longer experiments were also conducted). The obtained samples were subjected to sorption measurements using the Quantachrome Autosorb iQ instrument after degassing at different temperatures and  $10^{-6}$ - $10^{-7}$  mbar achieved vacuum (Tab. 5). All the samples except the copper compound **1** demonstrated practically non-existent capacities for nitrogen gas sorption and small, but non-negligible sorption hydrogen gas sorption at 77K (at least in comparison with other microporous materials). Increase of degassing temperature for the compound of zink, **2**, showed that the adsorbed amount of H<sub>2</sub> is passing through a maximum at 23.3 cm<sup>3</sup> (STP) of H<sub>2</sub> after degassing at 70°C *i.e.* indicating probable instability at higher temperature. The cadmium complex **2** indicated no increase of adsorbed hydrogen at higher degassing temperatures still leaving a chance that at app. 170-180°C a suitable conditions could be found (no deeper experimentation were done partially due to safety reasons implying possible explosion of the sensitized compound – a precaution which is seemingly excessive; the other reason was that the copper compound proved to be a better target for investigation regarding the ease of solvent exchange). No deeper investigation of the laminar manganese compound **4** was conducted because of lack of structural prerequisites for remarkable sorption phenomena.



**Fig. S26** The isolated **1** with app. crystal sizes at ~0.1 mm were subjected to solvent exchange (the sample was stored under inert gas, the photo is taken on air using a small batch sacrificed for that purpose).

The copper compound **1** (Fig. S26), demonstrating measurable mesoporosity after solvent exchange and activation, was subjected to additional solvent exchange experiments. It

was found that ~20-30 days of prolonged solvent exchange at room temperature with periodic change of the supernatant is roughly equivalent to ~5-10 days of exchange at 70°C. In both cases the material adopts a slightly different, more bluish coloration and deteriorates slightly according to microscopic inspection. The vessels containing the sample were purged by inert gas after every operation). It was found that the exchange depth was slowing down with time as witnessed by IR monitoring of prolonged exchange in MeOH (Fig. S18). Small amount of residual DMF solvent were invariably detected by IR spectroscopy at any conditions used.

During a typical sample preparation, the solvent exchanged material was filtered off, quickly washed with methanol a few times then dried at 1 Torr and room temperature. The pre-dried material was transferred in the sample tubes for sorption measurements and degassed at the ultimate vacuum at 30°C first and then at 70°C or 80°C using 0.5-1°C/min temperature rise rate. The colour of the sample changed from green to yellowish brown.

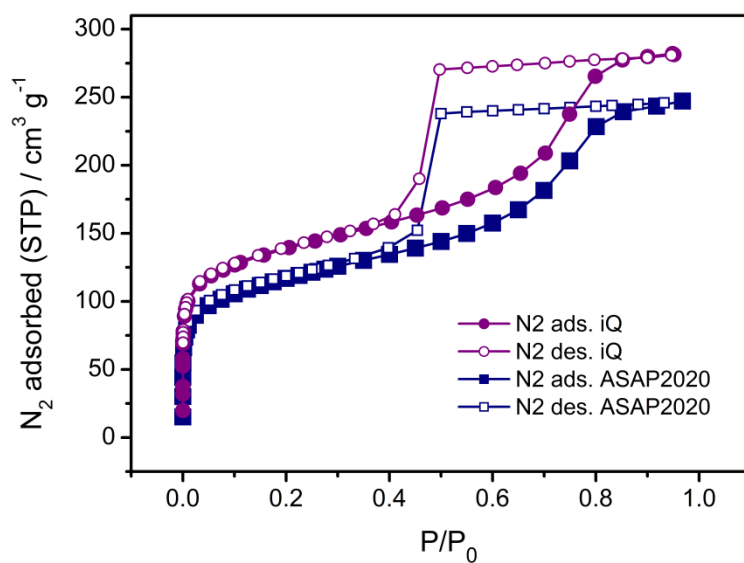


**Fig. S27** N<sub>2</sub> sorption isotherms at 77K measured by two different sorption analyzers on two independently prepared samples **1**.

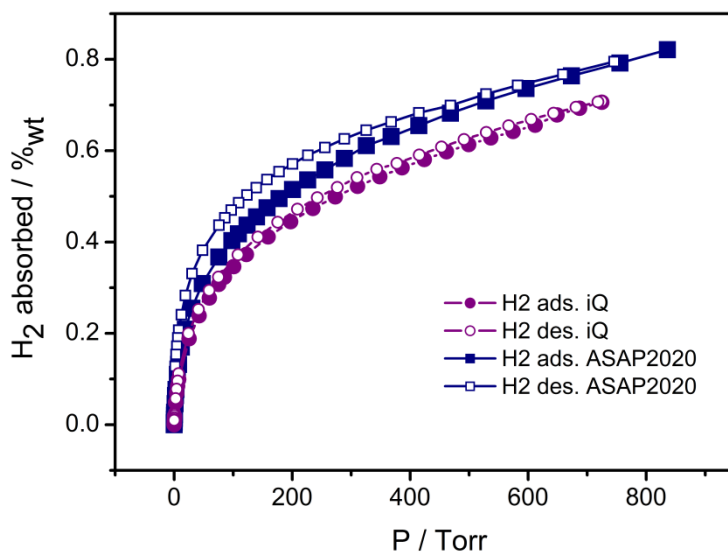


**Fig. S28** H<sub>2</sub> sorption isotherms at 77K measured by two different sorption analyzers on two independently prepared samples of **1**.

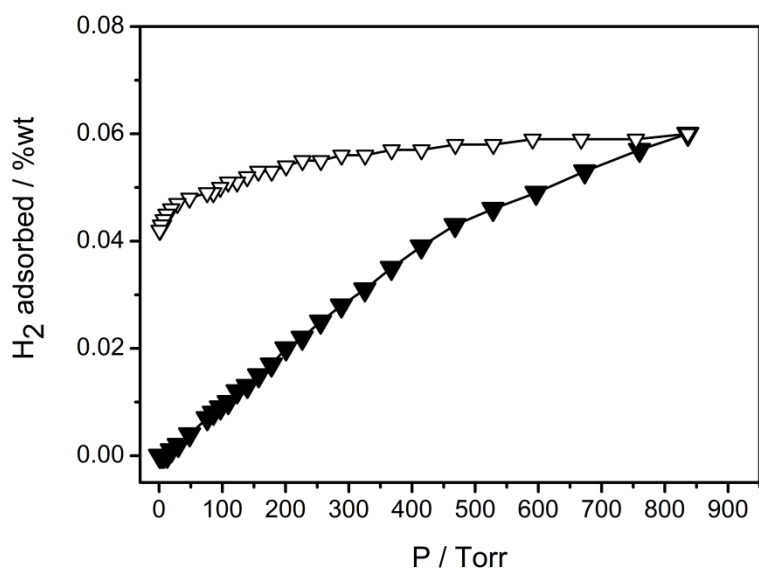


**Fig. S29** H<sub>2</sub> sorption isotherms at 20°C (Micromeritics ASAP 2020) for **1**. The amount of the adsorbed gas is small (~0.06 %<sub>wt</sub>), but the gas is trapped inside the pores and its escape is strongly hindered.

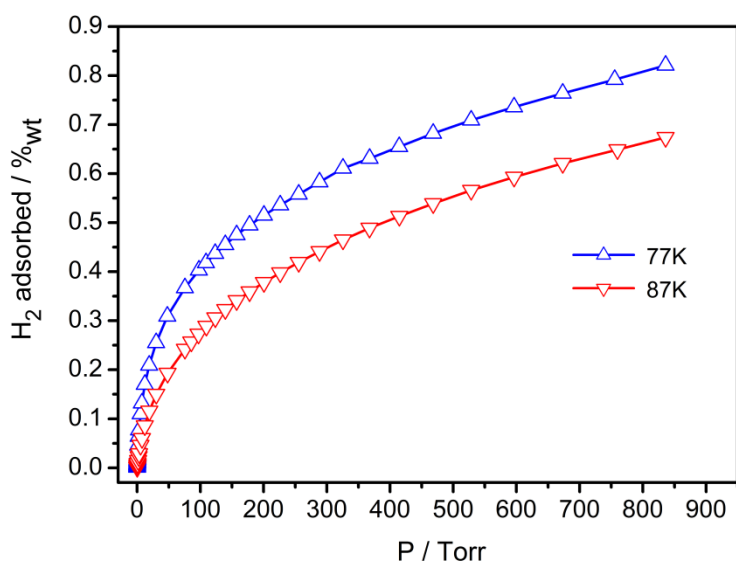


**Fig. S30** H<sub>2</sub> adsorption isotherms at 77K and 87K for **1** measured on Micromeritics ASAP 2020. 0.79 wt% H<sub>2</sub> adsorption at 760 Torr and 77K.

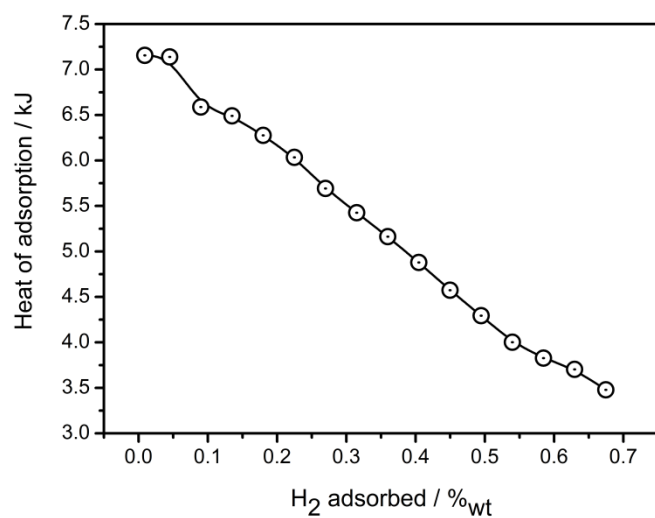
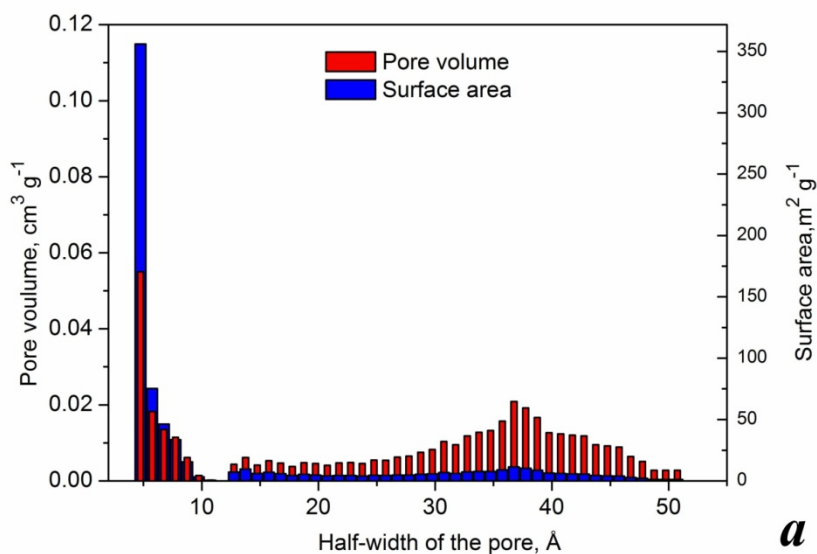
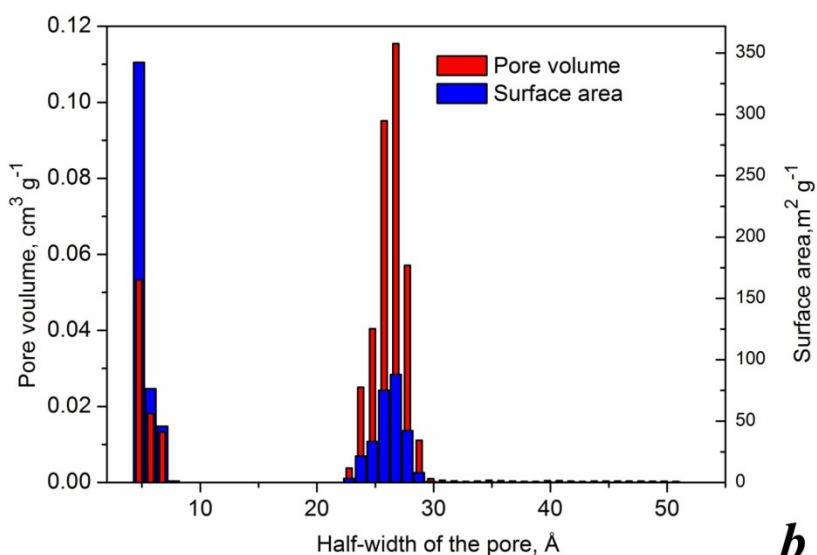


**Fig. S31** Heat of adsorption dependence upon amount of hydrogen adsorbed for **1**. The data is derived using Clausius-Clapeyron equation and isotherms measured at 77K ad 87K. The isosteric heat of adsorption at zero coverage is  $\sim 7.2$  kJ / mol.



**a**



**b**

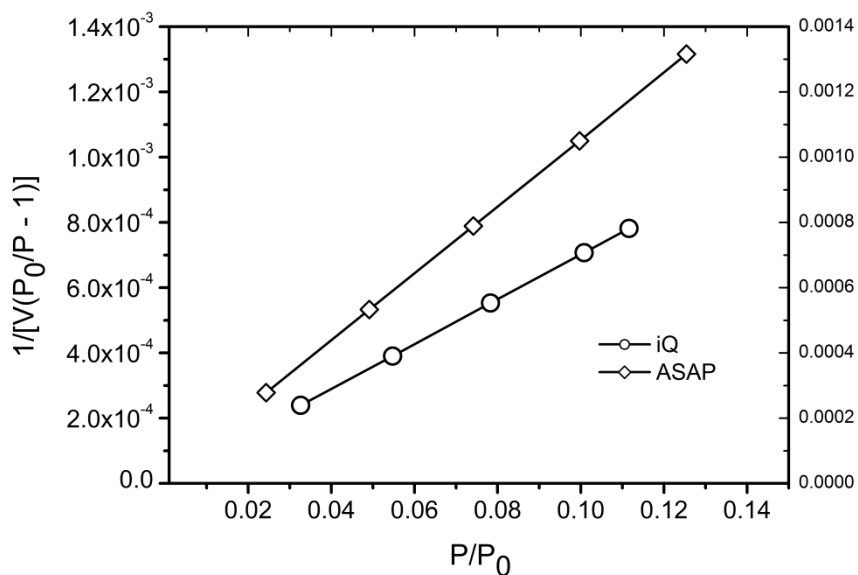
**Fig. S32** NLDFT calculations on the N<sub>2</sub> adsorption data (77K) collected by the iQ analyzer and using the native ASiQwin 2.0 software (Quantachrome Instruments).

a) Cylindrical pores, silica, adsorption branch (preferred for the H2 type adsorption isotherms).

b) Cylindrical pores, silica, equilibrium model (given for comparison with a), as both models are not precise in the case when structural transformations take place).

**Tab. S6** BET surface areas for two independent sorption analyzers on two independently prepared samples of **1**.

Quantachrome Autosorb-iQ			Micromeritics ASAP2020		
P/P <sub>0</sub>	V <sub>N<sub>2</sub></sub> (STP), cm <sup>3</sup> g <sup>-1</sup>	1/[V <sub>N<sub>2</sub></sub> (P <sub>0</sub> /P - 1)]	P/P <sub>0</sub>	V <sub>N<sub>2</sub></sub> (STP), cm <sup>3</sup> g <sup>-1</sup>	1/[V <sub>N<sub>2</sub></sub> (P <sub>0</sub> /P - 1)]
0.0326239e	112.8706	0.00023906	0.024337807	89.7872	0.000278
0.0547429	118.7458	0.00039022	0.049113610	96.8460	0.000533
0.0782980	122.9355	0.00055288	0.074164567	101.5686	0.000789
0.100800	126.8110	0.00070729	0.099735733	105.5516	0.001050
0.111559	128.5431	0.00078159	0.125416237	108.9376	0.001316
BET Surface Area = 505.474 m <sup>2</sup> g <sup>-1</sup> C = 478.086 Correlation coefficient, r = 0.9999			BET Surface Area: 423.1481 ± 0.8025 m <sup>2</sup> g <sup>-1</sup> C = 363.755980 Correlation Coefficient: 0.9999		



**Tab. S7** Data for N<sub>2</sub> adsorption isotherms (77K) measured on two independently prepared samples of **1** using two different sorption analyzer instruments.

Quantachrome Autosorb-iQ		Micromeritics ASAP2020	
P/P <sub>0</sub>	Quantity adsorbed STP, cm <sup>3</sup> g <sup>-1</sup>	P/P <sub>0</sub>	Quantity adsorbed STP, cm <sup>3</sup> g <sup>-1</sup>
5.37E-07	19.8241	5.42E-06	15.0966
3.45E-06	31.8778	1.26E-05	30.0757
6.93E-06	37.3971	8.16E-05	44.1009
4.88E-05	52.4551	3.59E-04	54.7513
7.23E-05	55.6638	0.00163	65.9991
9.55E-05	57.9104	0.00407	73.7748
3.69E-04	69.0908	0.00725	79.0302
5.73E-04	72.9961	0.0108	82.4556
8.02E-04	75.97	0.02434	89.7872
0.00101	78.0636	0.04911	96.846
0.00334	89.2333	0.07416	101.5686
0.00559	94.3445	0.09974	105.5516
0.00781	97.7145	0.12542	108.9376
0.01001	100.2481	0.15012	111.6715
0.03262	112.8706	0.17503	114.3315
0.05474	118.7458	0.2002	116.8914
0.0783	122.9355	0.2252	119.1026
0.1008	126.811	0.25021	121.3978
0.11156	128.5431	0.2751	123.6805
0.15671	134.0024	0.30029	125.8294
0.20612	139.4861	0.35016	130.1009
0.25605	144.2951	0.40039	134.5234
0.30545	148.9455	0.4504	139.1599
0.35512	153.6004	0.50038	144.0234
0.40418	158.3827	0.55005	149.8951
0.45341	163.362	0.6002	157.5239
0.5027	168.6999	0.65009	167.3382
0.55196	175.0805	0.69981	181.4909
0.60591	183.6912	0.74946	203.2132
0.65442	194.1464	0.80098	228.3986
0.70224	208.9504	0.8533	239.343
0.74935	237.5756	0.91769	243.4406
0.79908	265.3437	0.96793	247.1506
0.85158	277.3804	0.93221	245.9356
0.90043	279.8276	0.88183	244.7565
0.94876	281.9676	0.83157	243.9807
0.9514	281.3217	0.80023	243.3677
0.94649	280.9464	0.74999	242.4735
0.90009	279.165	0.70012	241.5813
0.85186	278.4312	0.65025	240.7838
0.79735	277.4997	0.60039	240.0292
0.74926	276.3239	0.55034	239.2674

0.70193	275.0135	0.50005	237.9756
0.64774	273.7859	0.45432	152.2699
0.5999	272.6981	0.39818	139.391
0.55141	271.6488	0.33265	131.5375
0.49731	270.4051	0.28202	126.4739
0.45793	190.0926	0.25643	124.0325
0.41088	163.8467	0.25021	123.3442
0.36923	156.967	0.22488	120.977
0.32389	151.7694	0.20018	118.7006
0.27911	147.4371	0.17514	116.4085
0.23445	143.0939	0.15008	114.0099
0.19023	138.7069	0.12509	111.3717
0.14585	133.8647	0.10009	108.3646
0.10066	128.1529	0.0751	104.8627
0.07723	124.4655	0.05177	100.6527
0.05492	120.215	0.02526	93.3101
0.03307	114.6212	0.01004	84.9584
0.00992	101.6846		
0.0077	99.0839		
0.00546	95.6239		
0.00325	90.5861		
9.47E-04	79.1944		
7.70E-04	77.2709		
5.31E-04	73.9675		
3.20E-04	69.5941		

**Tab. S8** Data for H<sub>2</sub> adsorption isotherms measured on two independently prepared samples of **1** using two different sorption analyzer instruments at 77K (L<sub>N2</sub>) and 87K(L<sub>Ar</sub>)

Quantachrome Autosorb-iQ, 77K			Micromeritics ASAP2020, 77K			Micromeritics ASAP2020, 87K		
Absolute pressure, Torr	Quantity adsorbed STP, cm <sup>3</sup> g <sup>-1</sup>	Weight %	Absolute pressure, Torr	Quantity adsorbed STP, cm <sup>3</sup> g <sup>-1</sup>	Weight %	Absolute pressure, Torr	Quantity adsorbed STP, cm <sup>3</sup> g <sup>-1</sup>	Weight %
0.0014	3.00E-04	2.70E-06	0.017586	-0.0433	0	0.18501	0.1112	1.00E-03
0.0026	6.00E-04	5.40E-06	0.056319	0.1374	0.001	0.39165	0.4447	0.004
0.0365	0.0841	7.56E-04	0.097811	0.3386	0.003	0.54781	0.5559	0.005
0.063	0.1525	0.00137	0.131103	0.4917	0.004	0.70386	0.7782	0.007
0.0881	0.1996	0.0018	0.175087	0.6941	0.006	0.86747	1.0006	0.009
0.3312	0.8934	0.00804	0.214749	0.8626	0.008	1.50832	1.6676	0.015
0.4283	1.1625	0.01046	0.248724	1.0077	0.009	2.36952	2.5570	0.023
0.6244	1.6775	0.01509	0.296449	1.2113	0.011	3.15415	3.2241	0.029
0.7932	2.0887	0.01879	0.337956	1.381	0.012	5.44263	5.1141	0.046
2.598	5.4237	0.04878	0.372834	1.5197	0.014	7.71658	6.6706	0.06
4.2797	7.6568	0.06887	0.408077	1.6571	0.015	12.10188	9.5611	0.086
5.8978	9.414	0.08468	0.443622	1.7917	0.016	19.40415	12.8964	0.116
7.6498	11.0198	0.09912	0.4792	1.9252	0.017	30.23179	16.6764	0.15
25.4078	20.9283	0.18825	0.529573	2.1124	0.019	48.08397	21.4570	0.193
42.1832	26.5268	0.2386	0.577065	2.2853	0.02	75.69069	26.9046	0.242
59.5857	30.8528	0.27751	0.622232	2.4453	0.022	85.66138	28.5723	0.257
75.3649	34.1705	0.30736	0.664508	2.5928	0.023	96.98634	30.3511	0.273
85.1309	35.9232	0.32312	0.703948	2.7278	0.024	109.5533	32.1299	0.289
101.069	38.4709	0.34604	0.741262	2.8528	0.025	123.5993	34.0199	0.306
122.3732	41.4309	0.37266	0.774602	2.962	0.026	139.5255	35.9099	0.323
159.3295	45.7146	0.41119	0.806564	3.0661	0.027	157.406	37.9110	0.341
197.3477	49.4382	0.44469	1.51769	5.1421	0.046	177.7227	39.9122	0.359
235.0865	52.6484	0.47356	2.39556	7.2028	0.064	200.5519	42.0246	0.378
272.9296	55.4735	0.49897	3.125883	8.6539	0.077	226.3464	44.2481	0.398
310.6728	58.0225	0.5219	5.517053	12.3028	0.11	255.4745	46.5828	0.419
348.54	60.3668	0.54299	7.57746	14.7798	0.132	288.3672	49.0287	0.441
386.0772	62.5386	0.56252	12.23203	19.0219	0.17	325.511	51.6969	0.465
423.8521	64.5541	0.58065	19.06453	23.4503	0.209	367.4338	54.3651	0.489
461.66	66.4287	0.59751	30.06839	28.5843	0.255	414.7494	57.0333	0.513
499.1868	68.1957	0.61341	47.74087	34.5831	0.309	468.1644	59.9239	0.539
536.7701	69.8251	0.62806	75.68233	41.1475	0.367	528.4306	62.9257	0.566
574.4418	71.3952	0.64218	97.73554	45.1399	0.403	596.4161	65.9274	0.593
612.0548	72.9161	0.65586	108.9564	46.8655	0.418	673.2682	69.0403	0.621
649.0917	75.4089	0.67829	123.5208	48.9906	0.437	759.978	72.1533	0.649
687.2162	77.0223	0.6928	139.5501	51.0372	0.455	835.9454	74.9327	0.674
724.8741	78.5043	0.70613	157.4528	53.1979	0.475			
724.3949	78.7538	0.70837	177.7355	55.4994	0.495			
718.3394	78.575	0.70676	200.6477	57.7015	0.515			
680.9953	77.2763	0.69508	226.3335	60.0834	0.536			
643.0618	75.8332	0.6821	255.5268	62.5784	0.558			
605.0807	74.3241	0.66853	288.4559	65.2849	0.583			
567.0889	72.7742	0.65459	325.5545	68.4413	0.611			
529.209	71.1369	0.63986	367.7511	70.6817	0.631			
491.2754	69.4267	0.62448	414.5295	73.4603	0.655			
453.3268	67.6175	0.6082	468.3155	76.4649	0.682			

415.3828	65.6705	0.59069	528.5114	79.4099	0.709
377.4008	63.6254	0.5723	596.4558	82.4577	0.736
343.3364	62.199	0.55947	673.3305	85.6093	0.764
309.9057	60.1768	0.54128	755.4957	88.7867	0.792
276.3156	57.7707	0.51963	836.0184	92.0154	0.821
242.5811	55.2677	0.49712	745.7032	89.066	0.795
208.9706	52.4651	0.47191	658.9094	86.0094	0.767
175.3883	49.3004	0.44345	582.1447	83.2673	0.743
141.8665	45.6847	0.41092	528.5341	81.1909	0.724
108.3036	41.3834	0.37223	468.3317	78.3932	0.699
74.9546	35.9353	0.32323	414.5955	76.5616	0.683
59.2629	32.6971	0.2941	367.6826	74.3043	0.663
41.0742	28.0558	0.25236	325.4836	72.2595	0.645
24.2961	22.2318	0.19997	288.4712	70.1249	0.626
7.4326	12.4249	0.11176	255.5157	68.0742	0.607
5.8907	10.647	0.09577	226.4186	66.0769	0.59
4.0766	8.646	0.07777	200.634	64.0455	0.571
2.4186	6.3468	0.05709	177.6524	62.1046	0.554
0.6694	2.9344	0.02639	157.1207	60.1468	0.537
0.5731	2.6728	0.02404	139.2301	58.2045	0.519
0.4141	2.2377	0.02013	123.2312	56.3281	0.503
0.216	1.6659	0.01498	109.2652	54.4421	0.486
0.0696	1.2364	0.01112	96.76365	52.6251	0.47
0.0372	1.1068	0.00996	85.76227	50.7576	0.453
			75.95747	48.9868	0.437
			48.14039	42.8141	0.382
			30.23517	37.0536	0.331
			19.03866	31.6874	0.283
			12.20805	27.046	0.241
			7.643533	23.1673	0.207
			6.112707	21.3248	0.19
			4.603573	19.2771	0.172
			3.223402	17.259	0.154
			1.602022	14.3704	0.128